Pergamon

Geochimica et Cosmochimica Acta, Vol. 66, No. 12, pp. 2073–2090, 2002

0016-7037/02 $22.00 + .00

PII S0016-7037(02)00890-6

Generation of mid-ocean ridge basalts at pressures from 1 to 7 GPa

DEAN C. PRESNALL,[1,2,*] GUDMUNDUR H. GUDFINNSSON,[1] and MICHAEL J. WALTER[3]

[1]Geophysical Laboratory, Carnegie Institution of Washington, Washington, D. C. 20015-1305, USA
[2]The University of Texas at Dallas, P.O. Box 830688, Richardson, TX 75083-0688, USA
[3]Institute for Study of the Earth's Interior, Okayama University, Misasa, Tottori-ken 682-0193, Japan

(*Received June* 7, 2001; *accepted in revised form March* 4, 2002)

Abstract—We propose a model for the generation of average MORBs based on phase relations in the CaO-MgO-Al_2O_3-SiO_2-CO_2 system at pressures from 3 to 7 GPa and in the CaO-MgO-Al_2O_3-SiO_2-Na_2O-FeO (CMASNF) system at pressures from ~0.9 to 1.5 GPa. The MELT seismic tomography (Forsyth et al., 2000) across the East Pacific Rise shows the largest amount of melt centered at ~30-km depth and lesser amounts at greater depths. An average mantle adiabat with a model-system potential temperature (T_p) of 1310°C is used that is consistent with this result. In the mantle, additional minor components would lower solidus temperatures ~50°C, which would lower T_p of the adiabat for average MORBs to ~1260°C. The model involves generation of carbonatitic melts and melts that are transitional between carbonatite and kimberlite at very small melt fractions (<0.2%) in the low-velocity zone at pressures of ~2.6 to 7 GPa in the CMAS-CO_2 system, roughly the pressure range of the PREM low-velocity zone. These small-volume, low-viscosity melts are mixed with much larger volumes of basaltic melt generated at the plagioclase-spinel lherzolite transition in the pressure range of ~0.9 to 1.5 GPa.

In this model, solidus phase relations in the pressure range of the plagioclase-spinel lherzolite transition strongly, but not totally, control the major-element characteristics of MORBs. Although the plagioclase-spinel lherzolite transition suppresses isentropic decompression melting in the CMAS system, this effect does not occur in the topologically different and petrologically more realistic CMASNF system. On the basis of the absence of plagioclase from most abyssal peridotites, which are the presumed residues of MORB generation, we calculate melt productivity during polybaric fractional melting in the plagioclase-spinel lherzolite transition interval at exhaustion of plagioclase in the residue. In the CMASN system, these calculations indicate that the total melt productivity is ~24%, which is adequate to produce the oceanic crust. The residual mineral proportions from this calculation closely match those of average abyssal peridotites.

Melts generated in the plagioclase-spinel lherzolite transition are compositionally distinct from all MORB glasses, but do not have a significant fractional crystallization trend controlled by olivine alone. They reach the composition field of erupted MORBs mainly by crystallization of both plagioclase and olivine, with initial crystallization of either one of these phases rapidly joined by the other. This is consistent with phenocryst assemblages and experimental studies of the most primitive MORBs, which do not show an olivine-controlled fractionation trend. The model is most robust for the eastern Pacific, where an adiabat with a T_p of ~1260°C is supported by the MELT seismic data and where the global inverse correlation of $(FeO)_8$ with $(Na_2O)_8$ is weak. Average MORBs worldwide also are well modeled. A heterogeneous mantle consisting of peridotite of varying degrees of major-element depletion combined with phase-equilibrium controls in the plagioclase-spinel lherzolite transition interval would produce the form of the global correlations at a constant T_p, which suggests a modest range of T_p along ridges. Phase-composition data for the CMASNF system are presently not adequate for quantitative calculation of $(FeO)_8$-$(Na_2O)_8$-$(CaO/Al_2O_3)_8$ systematics in terms of this model. The near absence of basalts in the central portion of the Gakkel Ridge suggests a lower bound for T_p along ridges of ~1240°C, a potential temperature just low enough to miss the solidus for basalt production at ~0.9 GPa. An upper bound for T_p is poorly constrained, but the complete absence of picritic glasses in Iceland and the global ridge system suggests an upper bound of ~1400°C. In contrast to some previous models for MORB generation that emphasize large potential temperature variations in a relatively homogeneous peridotitic mantle, our model emphasizes modest potential temperature variations in a peridotitic mantle that shows varying degrees of heterogeneity. Calculations indicate that melt productivity changes from 0 to 24% for a change in T_p from 1240 to 1260°C, effectively producing a rapid increase to full crustal thickness or decrease to none as ridges appear and disappear.

1. INTRODUCTION

Active debate on the petrogenesis of mid-ocean ridge basalts (MORBs) began when the first analyses of dredged samples were reported (Engel and Engel, 1964a, 1964b; Engel et al., 1965). As part of this debate (Kushiro, 2000), Presnall et al. (1979) and Presnall and Hoover (1984, 1987) developed a model based on phase relations in the CaO-MgO-Al_2O_3-SiO_2 (CMAS) system and some preliminary data in the CaO-MgO-Al_2O_3-SiO_2-Na_2O (CMASN) system. For model lherzolite in the CMAS system, they proposed that a cusp in the solidus at the plagioclase-spinel lherzolite transition also exists in some form in the more complex natural mantle composition. They suggested further that primitive MORBs or melts close in composition to primitive MORBs are generated by enhanced

* Author to whom correspondence should be addressed (presnall@gl.ciw.edu).

melting over a relatively small pressure range in the vicinity of the plagioclase-spinel lherzolite transition. However, Asimow et al. (1995) demonstrated in a very elegant and simple way that in the CMAS system, crystallization rather than enhanced melting must occur during isentropic ascent of mantle material through the plagioclase-spinel lherzolite transition. Subsequently, Asimow et al. (2001) used MELTS (Ghiorso and Sack, 1995) to calculate a negative solidus slope in the plagioclase-spinel lherzolite transition region (see Appendix), which would also require crystallization during isentropic decompression in this pressure range.

Major-element quantitative modeling of MORBs (Klein and Langmuir, 1987, 1989; McKenzie and Bickle, 1988; Kinzler and Grove, 1992a, 1992b; Langmuir et al., 1992) has been based on volatile-free phase relations. This simplification provides a good approximation of the lherzolite solidus curve at low pressures. However, at a model-system pressure of 2.6 GPa, CO_2 causes an abrupt lowering of the solidus temperature by 300°C and a strong change in the melting relations (Dalton and Presnall, 1998a, 1998b). Here we develop a preliminary model for MORB generation based on volatile-free phase relations at low pressures and vapor-undersaturated phase relations controlled by CO_2 at higher pressures. For low-pressure phase-equilibrium controls, we combine data from the CMAS-Na_2O (CMASN) (Walter and Presnall, 1994) and CMAS-FeO (CMASF) (Gudfinnsson and Presnall, 2000) systems to obtain a close approximation of phase relations in the plagioclase-spinel lherzolite transition region for the six-component system CaO-MgO-Al_2O_3-SiO_2-Na_2O-FeO (CMASNF) in the approximate pressure range of 1 to 1.5 GPa. As this system contains 98% of the composition of MORBs and 99% of the lherzolite source, it provides a significantly improved basis for modeling the melting behavior of the mantle at low pressures while maintaining the topological rigor of a model system. These phase relations, which are topologically very different from those in the CMAS system and deviate significantly from those calculated from the MELTS database (see Appendix), require melting during isentropic decompression through the plagioclase-spinel lherzolite transition. We argue that the most extensive melting occurs in the pressure range of this transition, but generation of basaltic melts at pressures above this transition in the spinel lhersolite field may also occur. To address issues of additional melt generation at very low melt fractions in the low-velocity zone at depths up to ~220 km, we use recent data for melting of model lherzolite in the system CMAS-CO_2 at pressures extending up to 7 GPa (Dalton and Presnall, 1998a, 1998b). The effects on trace element and isotopic signatures of a region of low degree melting at depths greater than the region of basalt production have been discussed elsewhere (e.g., McKenzie, 1985; Galer and O'Nions, 1986; Plank and Langmuir, 1992; Faul, 2001). We address here only the major-element issues.

2. SEISMIC CONSTRAINTS ON MELTING BENEATH RIDGES

The oceanic low-velocity zone has long been understood to be a region of partial melting at very low melt fractions (e.g., Lambert and Wyllie, 1968; Anderson and Sammis, 1970; Eggler, 1976). Directly beneath ridges, the upper boundary of the low-velocity zone is modified by the addition of a more shallow melt region related to the generation of MORBs. A detailed description of the depth range of melting beneath the East Pacific Rise is provided by S-velocity inversions of data from the MELT seismic experiment (MELT Seismic Team, 1998). A dominant feature of the Rayleigh wave tomographic cross-section across the ridge is a localized and flattened region of very low velocity (as low as 3.95 km/sec) ~150-km wide with an aspect ratio of 4 to 5 (width/depth) and centered at a depth of ~30 km directly beneath the ridge (Forsyth et al., 2000). This region has a broad tail of moderately low velocities (~4.05–4.10 km/sec) slanting westward ~300 km and downward to a depth of ~80 km, which may be related to unique conditions for the East Pacific Rise with incoming flow from the Pacific superswell to the west (MELT Seismic Team, 1998; Gaboret et al. 2000; D. R. Toomey et al., submitted). Love waves from a regional event indicate that the top of the very low velocity region is at a depth of ~20 km beneath the ridge axis (Dunn and Forsyth, 2001). The bottom of the low-velocity zone is less welldefined. Regional and global surface wave studies (Nishimura and Forsyth, 1989; Ekstrom, 2000) and body wave tomography in the MELT experiment (Toomey et al., 1998) indicate that low velocities continue to a depth of 150 to 200 km. Although seismic velocity anomalies are sensitive to the presence of melt and not to the rate of melt production, these results may be interpreted to indicate that a large amount of melting occurs over a relatively small depth range centered at ~30 km beneath the ridge axis and that smaller amounts of melting occur at greater depths extending to 150 km or more. We use this result to support the existence of a mantle adiabat beneath ridges that intersects the peridotite solidus in such a way that a major amount of melting occurs at shallow depths, yet very small amounts of melt are produced at greater depths in the low-velocity zone. This is a fundamental feature of our model.

3. CONTROLS ON THE DEPTH RANGE OF MELTING

Attempts to use phase-equilibrium data to constrain the depth range for the generation of MORBs have yielded a wide variety of results ranging from the shallow mantle in the vicinity of the plagioclase-spinel lherzolite transition (e.g., Kushiro, 1973; Presnall et al., 1979) to the deeper mantle at pressures up to 3 GPa (O'Hara, 1968) and over a wide range of pressures from 0.8 to 2.5 GPa (Falloon and Green, 1988) and 0.4 to 2.5 GPa (T_p = 1315–1475°C) (Kinzler and Grove, 1992a). Klein and Langmuir (1987, 1989) and Langmuir et al. (1992) proposed a range of short to long melting columns to explain global major-element systematics, with pressures at the beginning of melting ranging from 1.2 to 4 GPa (T_p = 1260–1500°C). McKenzie and Bickle (1988) chose a T_p of 1280°C (≤1.5 GPa) for generating the mean composition of MORBs and emphasized the uniformity of T_p for most ridges. However, they used an extremely wide T_p range of 1160 to 1480°C to explain the global systematics of Klein and Langmuir (1987).

On the basis of rare earth element patterns in abyssal peridotites, the presumed residues of MORB generation, Johnson et al. (1990) concluded that a close approach to fractional melting is required for the generation of MORBs. In a more recent review of this issue, Kelemen et al. (1997) found that while

Table 1. Comparison of melting reactions for model systems and natural compositions.

P(GPa)	Melting Interval	System	Melting Reaction (wt.%)	Reference
Spinel lherzolite				
1.1	Invariant	CMAS	36 opx + 55 cpx + 9 sp = 77 liq + 23 ol	[1]
1.1	12-22%	CMASN	34 opx + 56 cpx + 10 sp = 75 liq + 25 ol	[2]
1.15	12-22%	CMASF	26 opx + 63 cpx + 11 sp = 75 liq + 25 ol	[3]
1.0	mg#75-67	natural	35 opx + 59 cpx + 5 sp = 78 liq + 22 ol	[4]
1.0	~7-18%	natural	31 opx + 58 cpx + 11 sp = 82 liq + 18 ol	[5]
Garnet lherzolite				
5.1	Invariant	CMAS	7 ol + 75 cpx + 18 gt = 60 liq + 40 opx	[6]
5.0	20-32%	Natural	9 ol + 71 cpx + 20 gt = 43 liq + 57 opx	[7]

[1] Gudfinnsson and Presnall (1996); [2] Walter and Presnall (1994); [3] Gudfinnsson and Presnall (2000); [4] Kinzler and Grove (1992b); [5] Baker and Stolper (1994); [6] Weng (1997); [7] Walter (1998).

some fractional melting must occur, there is a range of possible mixed modes of melting (i.e., fractional plus batch) that can satisfy the depletions of rare earth elements in abyssal clinopyroxenes. A related issue is the porosity threshold required for melt migration. Minarik and Watson (1995) concluded that a carbonate melt in a lherzolite mantle with a grain size of ~1 mm would probably be interconnected at <0.05% melting, a value consistent with a porosity threshold for migration of ~0.1% (Faul, 2001). However, basalts have a larger threshold of ~1% (Faul, 2001). Because the MELT seismic data indicate a large amount of melt at shallow depths and an extensive region at greater depths with a smaller melt fraction, we use two sets of phase-equilibrium controls, one for extraction of large volumes of basaltic melt over a restricted depth range at the plagioclase-spinel lherzolite transition (~30–45 km) and another for extraction of very small amounts of carbonatitic-to-kimberlitic melt from a large depth range extending approximately to the lower boundary of the seismic low-velocity zone. This type of model is very similar to the melt configuration suggested by Faul (2001) to explain ^{230}Th excesses in MORBs and by McKenzie and Bickle (1988).

3.1. Phase-Equilibrium Controls at the Plagioclase-Spinel Lherzolite Transition

Table 1 shows that for spinel lherzolite and garnet lherzolite, melting reactions in the CMAS system are very similar to those in the more complex CMASN and CMASF systems and in natural peridotites. This demonstrates that phase relations in the CMAS, CMASN, and CMASF systems are powerful tools for clarifying the melting behavior of the mantle. As the simplest of these (the CMAS system) contains 89% of the composition of fertile mantle peridotite, 85% of the composition of basalts, and all of the major phases in peridotite (olivine, orthopyroxene, clinopyroxene, plagioclase, spinel, garnet), the ability of all three model systems to mimic natural melting behavior is not surprising. However, as Table 1 shows only melting reactions for large melt fractions in the natural compositions, the viability of the model systems is demonstrated only for this situation. Minor components found in peridotite but missing from the CMAS system can be concentrated in the minute amounts of melt produced just above the solidus of natural peridotite, which can strongly affect the earliest stages of melting. This difficulty is significantly mitigated by a migration threshold of 1% porosity for basaltic melts and the very close approach to natural compositions that can be achieved in the CMASNF system. Nevertheless, some caution in using the six-component phase relations is still needed.

The relevant phase relations are shown in Figures 1, 2, 3, and 4. In the CMAS system, the transition between plagioclase lherzolite and spinel lherzolite is marked by an invariant point in P-T space involving the phases forsterite, enstatite, diopside, anorthite, spinel, and liquid (Fig. 1). This point lies at 0.93 GPa (Walter and Presnall, 1994), a slight revision from the value of 0.9 GPa given by Presnall et al. (1979). The invariant point causes a cusp on the lherzolite solidus (Presnall, 1976; Presnall et al., 1979). For lherzolite compositions, the important univariant curves coming from this invariant point are the low-pressure solidus curve (opx + cpx + an = fo + liq), the high-pressure solidus curve (opx + cpx + sp = fo + liq), and the subsolidus transition (ol + an = opx + cpx + sp).

In the CaO-MgO-Al_2O_3-SiO_2-Na_2O (CMASN) system (Walter and Presnall, 1994), the low-pressure (plagioclase lher-

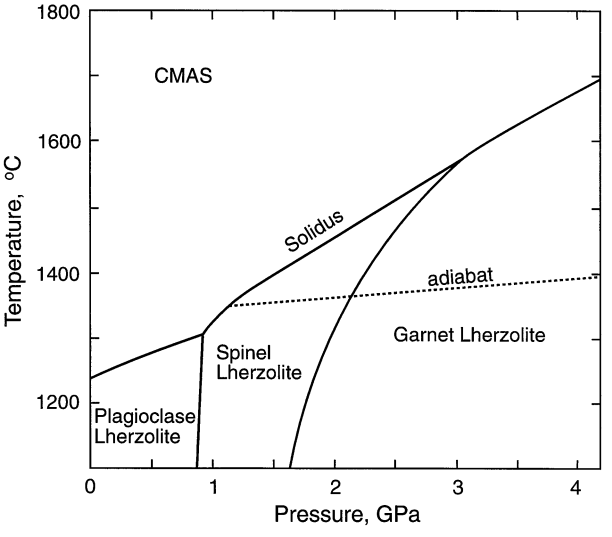

Fig. 1. Solidus and subsolidus phase relations for model lherzolite in the system CaO-MgO-Al_2O_3-SiO_2. Compiled from Davis and Schairer (1965), Kushiro and Yoder (1966), O'Hara et al. (1971), Herzberg and O'Hara (1972), Presnall (1976), Presnall et al. (1979), Gasparik (1984), Gudfinnsson and Presnall (1996), and Milholland and Presnall (1998).

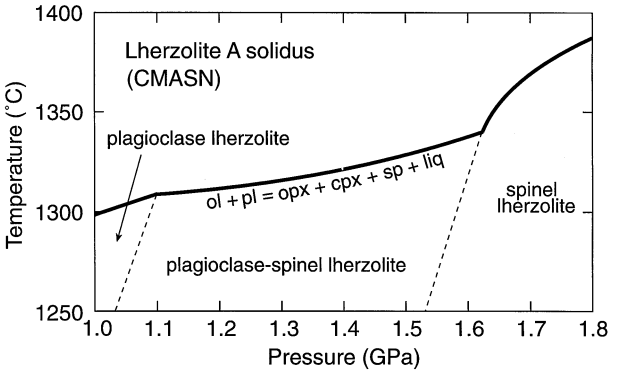

Fig. 2. Solidus (heavy solid line) for model lherzolite A in the CMASN system (revised from Walter and Presnall, 1994).

zolite) and high-pressure (spinel lherzolite) solidus curves become divariant solidus surfaces that descend to lower temperatures and meet along a univariant curve. This curve extends to higher pressures and temperatures from the invariant point on the CMAS solidus and involves the six-phase assemblage: ol + opx + cpx + pl + sp + liq (Walter and Presnall, 1994; Fig. 4). A singular point occurs on this curve at 1.05 GPa, where the reaction changes from fo + opx + pl = cpx + sp + liq at lower pressures to fo + pl = opx + cpx + sp + liq at higher pressures. The slope of this curve is nearly constant over the pressure range studied and produces a "ledge" on the model lherzolite solidus that corresponds to a pressure interval in which the subsolidus lherzolite assemblage (fo + opx + cpx) contains both plagioclase and spinel (Fig. 2).

In the CaO-MgO-Al_2O_3-SiO_2-FeO (CMASF) system, a univariant curve with a small positive dT/dP slope (Gudfinnsson and Presnall, 2000; Fig. 1) extends from the CMAS invariant point that produces a topology essentially identical to that in the CMASN system, including the occurrence of a singular point at a pressure between 0.93 and 1.1 GPa. The defining reactions for the curve on either side of the singular point have the same form as those in the CMASN system. Surprisingly, the addition

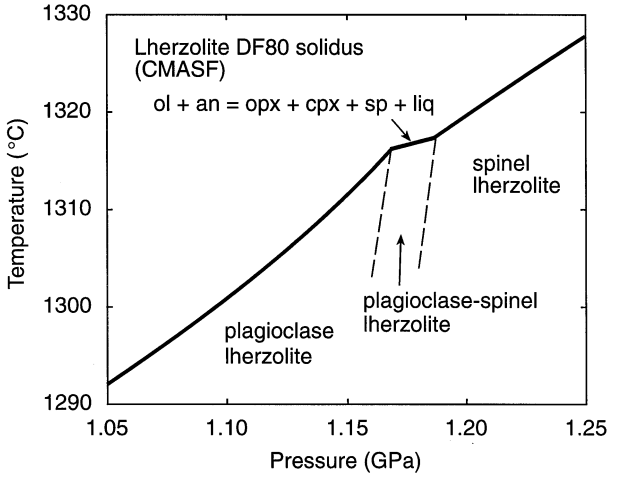

Fig. 3. Solidus (heavy solid line) for model lherzolite DF80 in the CMASF system (after Gudfinnsson and Presnall, 2000).

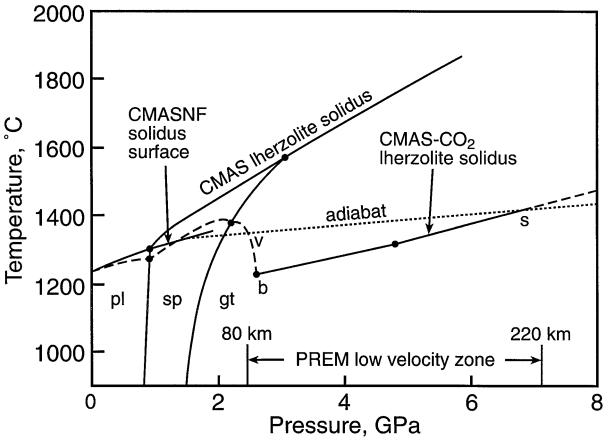

Fig. 4. Model CMAS lherzolite phase boundaries from Figure 1 with the CMAS-CO_2 lherzolite solidus and the CMASNF divariant solidus surface along which model plagioclase-spinel lherzolite would melt in six-space. Filled circles are invariant points. The model abiabat (potential temperature = 1310°C) has a slope of 15°C/GPa and is positioned so that it intersects the CMASNF solidus at 1.5 GPa. Pl, plagioclase lherzolite; sp, spinel lherzolite; gt, garnet lherzolite. Complied from Walter and Presnall (1994), Dalton and Presnall (1988a), Gudfinnsson and Presnall (2000), Dziewonski and Anderson (1981), and references given in the caption for Figure 1.

of FeO to the CMAS system acts in the same way as Na_2O in shifting the plagioclase-spinel lherzolite transition to higher pressures. Figure 3 shows the solidus for model lherzolite DF80 in the CMASF system, and for this composition, the width of the transition is much smaller than for model lherzolite in the CMASN system (Fig. 2).

The univariant solidus curves in Figures 2 and 3 form limiting boundaries for a divariant solidus surface in the CMASNF system. Temperature data are available for this surface only along its limiting edges (Figs. 2, 3), but because of the unexpected finding that the positions of the two limiting curves in P-T space are identical within experimental uncertainty, we assume the relatively safe approximation that points on the six-space solidus surface also lie within experimental uncertainty along the same P-T trajectory. Thus, the divariant CMASNF solidus surface is drawn as a single line in P-T space (Fig. 4), which means that isotherms and isobars on the surface, when viewed in composition space, are essentially parallel.

Data by Kinzler and Grove (1992b) on natural and synthetic compositions containing TiO_2, K_2O, MnO, and in some cases, Cr_2O_3 and P_2O_5, in addition to the CMASNF components, are shown in Figure 5. Within experimental error, their data in the pressure range 0.9 to 1.6 GPa can be described by a single line for the assemblage liq + ol + opx + cpx + sp + pl, with spinel absent below the line and plagioclase absent above. Because the slope of the line is poorly constrained by their data, it has been arbitrarily drawn to be identical to the slope of the CMASNF solidus curve. This slope is well within their experimental uncertainty, but a slightly steeper positive slope would produce a small improvement in the fit. Rotation in the opposite direction toward a negative slope, as indicated by MELTS and pMELTS (see Appendix), would degrade the fit. Thus, in this pressure range, the data indicate that complex compositions containing nine to 11 components mimic the behavior of the

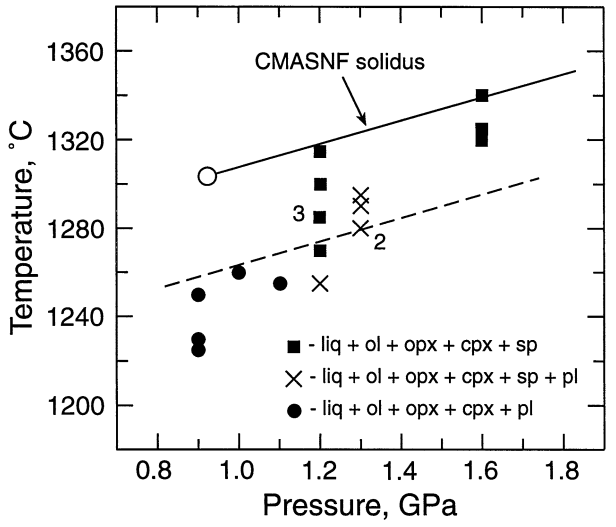

Fig. 5. Data of Kinzler and Grove (1992b) for runs that bracket the assemblage ol + opx + cpx + pl + sp + liq. Natural and synthetic starting compositions contain nine, 10, and 11 components. Numbers beside two points indicate number of experiments with the same result at identical conditions. Dashed line is a visual fit to the data with the slope arbitrarily set to match the CMASNF solidus slope (see text). Solid curve is the assemblage liq + ol + opx + cpx + pl + sp in the CMASNF system taken from Fig. 4. Open circle is the invariant point at the solidus between plagioclase- and spinel-lherzolite in the CMAS system. Temperature uncertainties are stated by Kinzler and Grove (1992b) to be ±15°C.

CMASNF solidus but at temperatures ~50°C lower. In addition, lowering the CMASNF model solidus by 50°C in this pressure range places it in agreement with the recommended mantle solidus of Hirschmann (2000) within his stated uncertainty of ±20°C. This agreement of the model system data with experiments on natural compositions further supports use of the CMASNF phase relations for modeling the generation of MORBs.

For natural lherzolite compositions at 0.2 to 0.5 GPa, Jaques and Green (1980), Takahashi and Kushiro (1983), Falloon et al. (1988), and Baker et al. (1995) found both plagioclase and spinel in equilibrium with olivine, orthopyroxene, clinopyroxene, and liquid. This indicates that for complex compositions, melting of lherzolite in the presence of both plagioclase and spinel extends to extremely low pressures. The details of these phase relations are not presently understood, but they are unlikely to be important in MORB generation (see section 8.3 below).

3.2. Phase-Equilibrium Controls in the Low-Velocity Zone

The need to consider very small melt fractions in the low-velocity zone presents a problem for experimental petrologists because of the difficulty in analyzing melts along narrow grain boundaries. In the most aggressive pursuit to date of small melt fractions of natural peridotite, Baker et al. (1995) were able to achieve direct analyses of liquids at 1 GPa for melt percentages down to 2% (see also Baker et al., 1996; Falloon et al., 1996; Hirschmann, et al., 1998). However, no melting studies exist on natural peridotites that combine the high pressures, extremely low melt fractions, and the effects of CO_2 appropriate for the low-velocity zone.

In a model-system approach, there is no difficulty in determining, without extrapolation, the compositions of arbitrarily small amounts of melt right down to the solidus. To understand melting behavior in the low-velocity zone, we use data in the system CMAS-CO_2 for model lherzolite along the solidus from 3 to 7 GPa and at 6 GPa for temperatures above the solidus (Dalton and Presnall, 1998a, 1998b). This system combines a good approximation of peridotite with the effect of CO_2 in producing extremely small melt fractions of carbonititic to kimberlitic composition at temperatures several hundred degrees below the CO_2-free solidus.

3.2.1. CO_2 controls on the solidus in the low-velocity zone

The existence of CO_2 throughout the upper mantle is indicated by the occurrence of carbonate-bearing kimberlites on continents worldwide, the occurrence of carbonatites in both oceanic (Allègre et al., 1971; Silva et al., 1981; Kogarko, 1993; Hauri et al., 1993) and continental environments, the unfailing occurrence of CO_2 inclusions in all olivine-bearing mantle xenoliths worldwide (Roedder, 1965, 1984), and the presence of CO_2 in the eruptive gases of volcanoes in both oceanic and continental regions. In one well-documented example, Gerlach and Graeber (1985) and Gerlach et al. (2001) determined that the primary magma at Kilauea volcano in Hawaii contains 0.7% CO_2. Le Bas (1984) argued that carbonatites would be much more abundant on oceanic islands if their plutonic basements were more commonly exposed by erosion.

As discussed most recently by Dixon and Clague (2001), CO_2 is relatively insoluble in melts at low to moderate pressures. During upward transport and eruption of magmas, a large proportion of the CO_2 boils off to form vesicles and is lost as escaping vapor. Dixon and Clague (2001) estimated that for Loihi seamount in Hawaii, >99% of the CO_2 is lost in this way. MORBs erupted under greater water pressures on the ocean floor do not escape this process, as indicated by the fact that 95% of the gas in MORB vesicles is CO_2 (Moore et al., 1977). Therefore, determination of the concentration of CO_2 in the upper mantle based on concentrations in lavas would be expected to give low and unreliable values. However, a reasonable estimate may be 170 to 430 ppm (Zhang and Zindler, 1993), which is based on the C/^{3}He outgassing ratio at mid-ocean ridges and total ^{3}He in the present degassed mantle.

Because the solubility of CO_2 in silicate melts is relatively small at low pressures, depression of the solidus is small. Carbon dioxide is present as vapor just below the solidus. At higher pressures (>2.6 GPa in the CMAS-CO_2 system; Fig. 4), CO_2 forms dolomite or magnesite just below the solidus, and the solidus melt is carbonatite, a melt composition close to that of the low-melting phases, dolomite (<4.8 GPa in the CMAS-CO_2 system) and magnesite (>4.8 GPa). In such a melt, the solubility of CO_2 is very high and depression of the solidus is correspondingly large. This accounts for the precipitous decrease in the temperature of the lherzolite solidus in the CMAS-CO_2 system at 2.6 GPa (Fig. 4), in which the decarbonation reaction, clinopyroxene + olivine + garnet + CO_2 = dolomite + orthopyroxene (Dalton and Presnall, 1998a), intersects the

solidus at invariant point b (Fig. 4) and stabilizes dolomite at higher pressures. As the solidus in CMAS-CO_2 is a univariant curve, its position in P-T space remains independent of the amount of CO_2. At P >2.6 GPa, the carbonate phase is absent at temperatures immediately above the solidus, and all CO_2 is dissolved into the melt. Therefore, the amount of melt that can be produced at the solidus depends directly on the amount of CO_2 in the unmelted source.

The depths at which the adiabat in Figure 4 crosses the CMAS-CO_2 solidus are similar to the upper and lower boundaries of the PREM low-velocity zone, although the depths of these boundaries vary. This is consistent with the idea that the solidus curve in this zone is controlled by the presence of CO_2, an explanation for the low-velocity zone also proposed much earlier on the basis of data in the simpler system, CaO-MgO-SiO_2-CO_2 (Eggler, 1975, 1976; Wyllie and Huang, 1975, 1976).

In the systems CaO-MgO-SiO_2-CO_2 and CaO-MgO-SiO_2-CO_2-H_2O, Wyllie (1977) and Eggler (1978) found that initial melts at high pressures are carbonatitic. Dalton and Presnall (1998a) also found carbonatite melts at the solidus in the system CMAS-CO_2 under vapor-undersaturated conditions and showed that this result persists up to at least 7 GPa. In addition, Dalton and Presnall (1998b) found that at 6 GPa the melt composition in equilibrium with lherzolite changes gradationally to a kimberlitic composition at ~150°C above the solidus. The existence of carbonatites but not kimberlites in the ocean basins supports the existence of low-temperature mantle adiabats in oceanic areas that lie close enough to the solidus to avoid the formation of kimberlites, a result consistent with our modeling.

3.2.2. *Adjustment of the CMAS-CO_2 solidus for additional minor components*

At 3.0 GPa, Wendlandt and Mysen (1980) located the vapor-undersaturated solidus of a natural peridotite + CO_2 at ~1120°C, which is ~130°C below the CMAS-CO_2 solidus at this pressure (Fig. 4). We take this as an approximate measure of the adjustment needed to shift the CMAS-CO_2 solidus in Figure 4 to temperatures appropriate for the more complex composition of the mantle. However, some uncertainty exists because the solidus of Falloon and Green (1989) is ~10°C below that of Wendlandt and Mysen (1980). The data of Falloon and Green (1989) indicate that the position of the subsolidus decarbonation reaction extending from b (Fig. 4) is not significantly changed by the addition of minor components. In this case, its intersection with the natural peridotite + CO_2 solidus of Wendlandt and Mysen (1980) would lie at ~2.3 GPa and 1120°C (not shown).

3.2.3. *Uncertain effect of H_2O on the solidus in the low-velocity zone*

The amount of H_2O in MORB glasses increases systematically with various indicators of fractional crystallization (Byers et al., 1984, 1986; Michael, 1988; Dixon et al., 1988), which supports a magmatic origin for the water found in the least-fractionated glasses. Michael (1988, 1995) gave values of 800 and 2100 ppm for least-fractionated N-MORB (normal trace elements) and E-MORB (enriched trace elements) glasses, respectively. Given a bulk partition coefficient for H_2O of 0.01 (Dixon et al, 1988), ~30% olivine + plagioclase fractionation of the most primitive MORBs to reach their observed compositions (see section 7, below), and ~15% melting at the source, the H_2O content of the mantle source would be ~90 ppm and ~230 ppm, respectively, for N-MORBs and E-MORBs. These estimates are slightly lower than those of Michael (1988) (100 ppm for N-MORBs and 350 ppm for E-MORBs) due to different modeling assumptions.

Given that a very small amount of water is present in the MORB mantle, its effect on melting behavior depends on its solubility in nominally anhydrous mantle phases. Small amounts of H_2O have been found, up to 140 ppm in olivine, 460 ppm in orthopyroxene, 590 ppm in clinopyroxene, and 200 ppm in garnet (Bell and Rossman, 1992). Experimental data on the maximum solubility of H_2O in these phases at high temperatures and pressures are sparse and sometimes in disagreement (Kohn, 1996; Kohlstedt et al., 1996; Withers et al., 1998; Matveev et al., 2001), and issues regarding analytical methods and appropriate experimental procedures are not settled. In addition, the solubility often increases with pressure, but not always (Kohlstedt et al., 1996; Withers et al., 1998). The extremes of low and high values, where available, suggest that the maximum bulk solubility in garnet lherzolite may lie somewhere in the range of 100 to 900 ppm for temperatures near 1000°C and various high pressures. However, the observed maximum bulk concentrations given by Bell and Rossman (1992) of 290 and 245 ppm for spinel lherzolite and garnet lherzolite, respectively, indicate that the lower solubility limit of 100 ppm may be too small. The minerals analyzed by Bell and Rossman (1992) are from xenoliths sampled by continental kimberlites, a mantle environment that is probably more enriched in H_2O than an oceanic ridge mantle. Although there are many uncertainties, the data suggest that the amount of H_2O in the MORB mantle can be dissolved in nominally anhydrous phases at values ranging from near the bulk saturation limit to about an order of magnitude less than the bulk saturation limit. If the amount of H_2O exceeds its bulk solubility limit, it could contribute to lowering of solidus temperatures even below those produced by CO_2. However, most of the data indicate that H_2O concentrations are significantly less than the bulk solubility limit at temperatures close to those of the peridotite + CO_2 solidus. In this case, which we assume here, the solidus would be controlled by CO_2. If further studies resolve the issue of maximum solubility in favor of low values, then the only change to the modeling in this paper would be a lower solidus at high pressures and slightly larger melt fractions in the low-velocity zone.

4. MELTING IN THE LOW-VELOCITY ZONE

4.1. Isentropic Equilibrium Melting

To evaluate melting in the low-velocity zone, we first consider the case of isentropic decompression melting under equilibrium conditions without any separation of melt from the residue. At depths >~220 km for a model mantle consisting of carbonated lherzolite in the CMAS-CO_2 system, magnesite would be the carbonate phase and only a very small amount of

it would be present. After intersecting the CMAS-CO_2 solidus at s (Fig. 4), the melting path extends only a very short distance along the univariant solidus curve, because magnesite, which would be present only in very small amounts, is the first phase to be exhausted by the production of a magnesiocarbonatite melt (Dalton and Presnall, 1998b). On exhaustion of magnesite, the melting path leaves the solidus curve and extends toward v. Between s and v, the path lies at most ~100°C above the CMAS-CO_2 solidus, and this occurs at ~2.6 GPa. If the amount of CO_2 in the mantle is known, then the data of Dalton and Presnall (1998b) can be used to calculate the amount of melt at various temperatures above the solidus at 6 GPa, a result expected to be similar all along the CMAS-CO_2 solidus from 3 to 7 GPa. A value of 200 to 400 ppm CO_2 in the mantle gives ~0.04 to 0.08% melting at the solidus and ~0.1 to 0.2% melting at ~100°C above the solidus at 6 GPa. As an approximation, we assume that these calculations also hold at 2.6 GPa, where the adiabat lies ~100°C above the solidus. Because of such a small amount of melting, the adiabat between s and v has been drawn with the same slope as that of a solid adiabat and with no deflections where it crosses the solidus.

At v (Fig. 4), the melting path encounters a univariant curve whose position has not been precisely determined but which has the reaction (wt.), 37 ol + 47 cpx + 4 gt + 12 CO_2 = 74 opx + 26 liq (Dalton and Presnall, 1998a) where it meets invariant point b. Therefore, the melt crystallizes as it moves along the path a very short distance up-temperature along the univariant curve. Carbon dioxide boils off as vapor, and the remaining melt reacts with opx to produce olivine, cpx, and garnet. However, complete crystallization is an artifact of phase relations in a system that is too simplified. As described below, further melting at lower pressures is evaluated using the CMASNF system, and our discussion of melting as a function of pressure, therefore, has a conceptual discontinuity in the pressure range of ~1.6 to 2.4 GPa. Because melting in the CMASNF system at pressures from ~1.0 to 1.6 GPa occurs at lower temperatures than in the CMAS system (Fig. 4), melting in the CMASNF-CO_2 system, for which no data exist, would also occur at similarly lower temperatures than those on the CMASNF solidus. That is, the solidus for the CMASNF-CO_2 system is expected to lie below the adiabat at all temperatures but closely approach the adiabat at ~2 GPa. Therefore, although the amount of melt at pressures just below v is expected to decrease for a model lherzolite in the CMASNF-CO_2 system, complete crystallization to produce two distinct melt zones beneath spreading ridges is not expected. Instead, a short interval of reduced melting would occur (Presnall, 1980). Melts from the normal part of the low-velocity zone would be able to pass into the low-pressure melting zone and mix with these lower-pressure basaltic melts, a result consistent with the MELT tomographic cross section across the East Pacific Rise (Forsyth et al., 2000).

4.2. Polybaric Fractional Melting

Perfect fractional melting implies separation of melt from the source as soon as it is formed. Although this case is a useful conceptual endmember, it is never realized in nature, because all physically realistic melting processes must have a porosity threshold for migration. In addition, as pointed out by Asimow et al. (1995, 2001), this kind of melting is not isentropic, because the departing melt takes entropy with it. We start by considering the consequences of a polybaric fractional melting process in which the only entropy change is the entropy carried away with the melt. Then we modify the process to include a porosity threshold for migration.

In Figure 4, a polybaric fractional melting path for ascending mantle material would begin in the same way as in equilibrium melting. The path would extend a very short distance along the solidus near point s and then leave the solidus curve when magnesite is exhausted. At this point, removal of the last bit of melt would also remove the last trace of CO_2 from the source, which would cause the solidus temperature of the residue to increase abruptly by ~550°C (Fig. 4). Then on further isentropic decompression, no further melting would occur until convective transport of the residue to the volatile-free CMASNF solidus at ~1.5 GPa. However, this result ignores the threshold porosity for melt migration. When such a threshold porosity (~0.1%; Faul, 2001) exists, the parcel of mantle would rise isentropically with no separation of melt until the growing melt volume exceeds the porosity threshold at some point between s and v. Thus, melts separated from the upper part of the low-velocity zone would dominate volumetrically over those separated from the lower part. Since carbonatitic melts on the solidus in the low-velocity zone would change gradationally toward kimberlitic compositions at roughly 150°C above the solidus, the adiabat drawn in Fig. 4 suggests that compositions of melts contributed to MORBs from the low-velocity zone would range from carbonatite to compositions intermediate between kimberlite and carbonatite with SiO_2 contents ranging from ~6 to 20% (Dalton and Presnall, 1998b). As the extractable melt fraction would be ~0.1%, these melts would contribute only in a minor and probably undetectable way to the major element composition of the much more voluminous basaltic melts generated at shallower depths at the plagioclase-spinel lherzolite transition. However, modeling of trace elements would need to consider melting processes in the low-velocity zone. Richardson and McKenzie (1994) calculated that the amount of melt contributed to MORBs from a garnet lherzolite source is limited to ~0.3%, which is generally consistent with the phase-equilibrium constraints used here.

5. MELTING AT THE PLAGIOCLASE-SPINEL LHERZOLITE TRANSITION

To show the relationship between MORBs and melts produced on the CMASNF divariant solidus surface at the plagioclase-spinel lherzolite transition, we use the extensive worldwide data of Melson (1992) for MORB glasses with ages <1 my. Use of this dataset has the advantage of eliminating scatter caused by interlaboratory analytical differences. Figure 6 shows projections of these MORB glass compositions and Figure 7 shows a primitive subset of these glasses. Even though small changes in Na_2O have a strong and well-known effect on the locations of points plotted in these diagrams, the primitive glasses lie in a fairly restricted region near the low-SiO_2 end of the MORB array.

Liquids on the CMASNF surface, the solidus in six-space for plagioclase-spinel lherzolite, are in equilibrium with olivine, orthopyroxene, clinopyroxene, plagioclase, and spinel. Figure 8

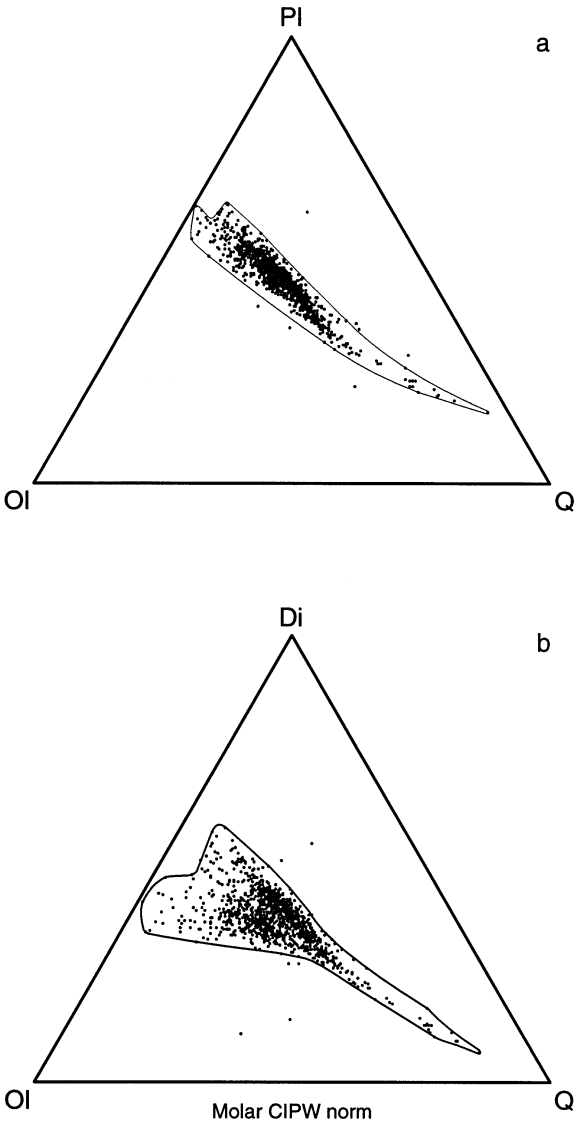

Fig. 6. Data of Melson (1992) for 1232 microprobe analyses of MORB glasses with ages <1 my plotted in the Di-Pl-Ol-Q tholeiitic basalt tetrahedron. (a) Projected from Di onto the Pl-Ol-Q face. (b) Projected from Pl onto the Di-Ol-Q face. For all analyses, $Fe^{2+}/(Fe^{2+} + Fe^{3+})$ is normalized to 0.91, the approximate maximum value found from wet chemical analyses of MORB glasses (Presnall et al., 1979; Fig. 11). Eleven ne-normative glasses are omitted. The outlines are drawn to reflect the form of the main concentration of points and to omit only the most extreme outliers. The procedure for calculating normative proportions is identical to the CIPW norm procedure except that minerals are in molar proportions, hy is calculated as equivalent ol and q, and ne-normative compositions appear as having negative q. The algorithm in molar amounts is:

$$Pl = Al_2O_3 - K_2O$$

$$Di = CaO + K_2O + Na_2O - 3.33P_2O_5 - Al_2O_3$$

$$Ol = (MgO + FeO + MnO + 3.33P_2O_5 + Al_2O_3 - TiO_2 - Cr_2O_3 - Fe_2O_3 - CaO - K_2O - Na_2O)/2$$

$$Q = SiO_2 - 5.5(K_2O + Na_2O) - 0.5(Al_2O_3 + MgO + FeO + MnO - TiO_2 - Fe_2O_3) - 1.5CaO + 5P_2O_5$$

.

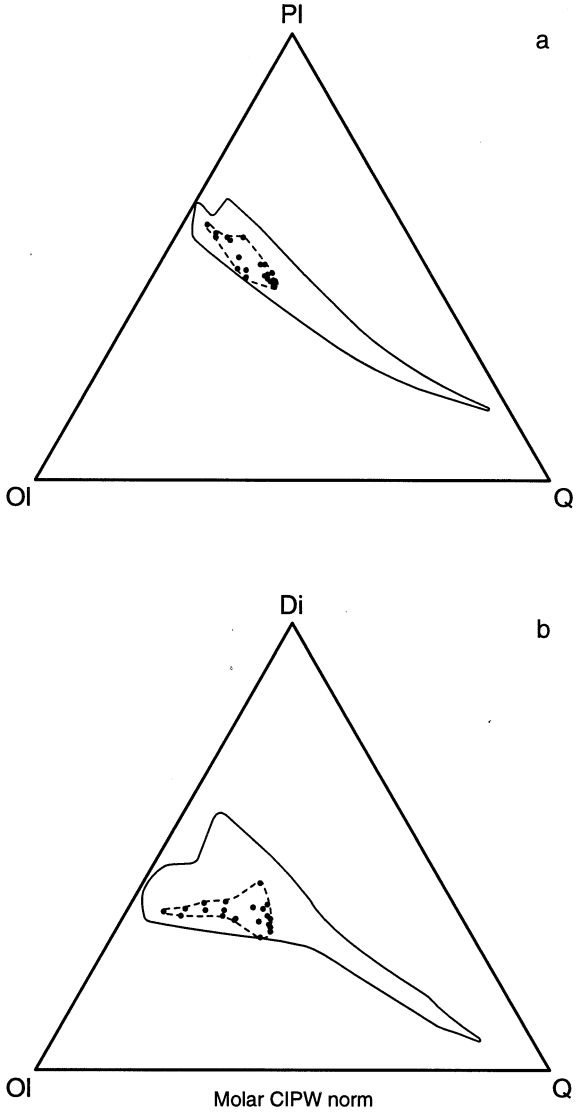

Fig. 7. Projections as in Figure 6 showing the 21 most primitive MORB glasses from Melson (1992) with mg numbers of 68 or greater (total Fe calculated as FeO). One omitted analysis is ne-normative.

shows the surface plotted in the tholeiitic portion of the basalt tetrahedron, Di-Pl-Ol-Q. Compositions of liquids on this surface have been determined only along the two boundaries, one where FeO is zero (Walter and Presnall, 1994) and the other where Na_2O is zero (Gudfinnsson and Presnall, 2000). Based on these data, estimated contours are shown for FeO and Na_2O, which must be subparallel to the two boundaries. For reference, an isobar is shown at 1.3 GPa, and isotherms would be approximately parallel to the isobars. In Figure 8a, the region of primitive MORBs appears to overlap the area of the CMASNF surface, but Figure 8b shows that it does not. Thus, if our model for generation of primitive MORBs on the CMASNF surface is correct, none have reached the Earth's surface unmodified by fractionation. The very large number and worldwide distribution of basalts in the Smithsonian database, combined with the closeness with which the CMASNF system approximates natural compositions, makes this conclusion firm.

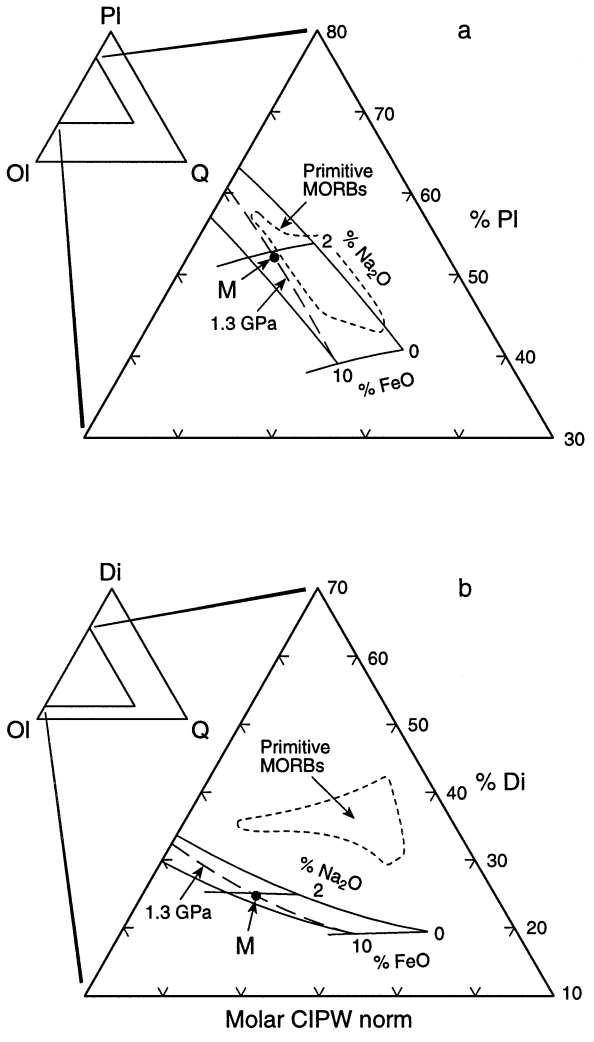

Fig. 8. Divariant surface in the CMASNF system for liquids in equilibrium with ol, opx, cpx, pl, and sp. Projections are the same as in Fig. 6. Point M is a model MORB parental liquid on the CMASNF divariant surface. Experimental data from Walter and Presnall (1994) and Gudfinnsson and Presnall (2000). Primitive MORB field from Fig. 7. Oxide contours are in wt.%.

6. MELT PRODUCTIVITY

As the plagioclase-spinel lherzolite solidus in the CMASNF system has a positive slope, intersection of an adiabat with this surface would produce melting during isentropic decompression. The absence of phase-composition data prevents isentropic melt productivity calculations at this time. As a proxy for this surface, productivity could be calculated using known phase compositions along the corresponding curve in the simpler CMASN system (Walter and Presnall, 1994) and entropy data from MELTS (Ghiorso and Sack, 1995) or pMELTS (M. S. Ghiorso et al., submitted). We are unable to do even this in an internally consistent way, because both of these databases show the solidus in the plagioclase-spinel lherzolite transition interval to have a negative dT/dP slope (see Appendix). Such a slope implies crystallization on intersection of the solidus during isentropic decompression rather than melting. In addition, the plagioclase-spinel lherzolite transition calculated from either MELTS or pMELTS occurs at roughly half the pressure indicated by our experimental data (see Appendix).

Table 2. Polybaric fractional melting of lherzolite A at plagioclase-spinel lherzolite transition in CMASN system.[1]

P(GPa)	wt.% Melt at Pl-out	wt.% Melt Extracted
1.5	2.1	1.1
1.4	2.5	1.5
1.3	2.6	1.6
1.2	2.8	1.8
1.1	3.4	2.4
1.0	5.5	4.5
0.95	12.0	11.0
Total Melt Extracted: 23.9%		
Aggregate Melt Composition (wt.%):		
CaO	13.8	
MgO	13.7	
Al_2O_3	20.9	
SiO_2	50.3	
Na_2O	1.3	
Residual Mineralogy (wt.%):		
Forsterite	77	
Orthopyroxene	20	
Clinopyroxene	3	
Average Plagioclase-free Abyssal Peridotite (vol.%):[2]		
Olivine	75	
Orthopyroxene	21	
Clinopyroxene	3.5	
Spinel	0.5	

[1] Calculated from data in Walter and Presnall (1994).
[2] From Dick et al. (1984).

As a substitute for the thermodynamically based calculation, we use the observation of Dick (1989) that roughly 80% of abyssal peridotites, which are generally understood to be the residues of MORB separation from the mantle, contain no plagioclase. In the remaining 20%, the plagioclase is considered to be the result of crystallization of trapped basaltic melt (Dick, 1989, and references therein). Thus, if MORBs are generated along the natural equivalent of the plagioclase-spinel lherzolite solidus surface in the CMASNF system, melting progresses to the point of plagioclase exhaustion. This is consistent with the observation that neither abyssal peridotites nor the less-fractionated MORBs show a significant Eu anomaly (Saunders, 1984; Johnson et al., 1990).

Table 2 shows a polybaric fractional melting calculation for lherzolite A in the CMASN system (Walter and Presnall, 1994). Melting is assumed to start at 1.5 GPa, which lies within the plagioclase-spinel lherzolite transition at the solidus (Fig. 2), and proceeds to the exhaustion of plagioclase at each 0.1-GPa step. To account for a threshold porosity for migration of 1% (Faul, 2001), only melt in excess of this threshold is extracted at each step. The retained 1% melt is recombined with the crystalline residue as part of the bulk composition melted in the next step.

Although the calculation omits FeO, the total amount of melt produced (24%; Table 2) is not expected to differ significantly from a calculation including FeO. This very high melt produc-

Table 3. Model upper mantle compositions.

	Lherzolite A (CMASN)[1]	Lherzolite DF80 (CMASF)[2]	Pyrolite[3]	Primitive Upper Mantle[4]
SiO_2	46.1	44.15	45.1	45.96
Al_2O_3	6.4	5.46	4.6	4.06
FeO[5]		7.98	7.9	7.54
MgO	43.0	38.48	38.1	37.78
CaO	4.2	3.94	3.1	3.21
Na_2O	0.3		0.4	0.33
Others			0.84	1.12

[1] Gudfinnsson and Presnall (2000).
[2] Walter and Presnall (1994).
[3] Ringwood (1975), Table 5-2.
[4] Hart and Zindler (1986).
[5] Total Fe as FeO.

tivity at low pressures is consistent with modeling of MORB generation based on trace element characteristics of Hawaiian xenoliths considered to be residues of magma generation beneath an oceanic ridge (Yang et al., 1998). The calculation indicates that melting along the plagioclase-spinel lherzolite transition is adequate to generate the oceanic crust. As pressure decreases, continuous extraction of melt progressively depletes the residue so that plagioclase in the residue becomes strongly enriched in anorthite, and the low-pressure boundary of the plagioclase-spinel lherzolite transition assemblage at the solidus (Fig. 2) is progressively reduced in pressure to accommodate the changing bulk composition of the source. As the Na_2O contents of melts produced in the final stages of melting are very low, we suggest that the An_{90-94} plagioclase megacrysts and phenocrysts found in some MORBs (Bryan et al., 1976; Donaldson and Brown, 1977; Stakes et al., 1984; Natland, 1989) are the product of a close approach to the end stages of fractional melting. Table 3 shows that the residual mineralogy contains only 3% clinopyroxene, and both plagioclase and spinel are exhausted. The nearly simultaneous loss of plagioclase and spinel moves the residue to a new region of the solidus where only olivine, orthopyroxene, and clinopyroxene coexist, and the solidus temperature is increased. Therefore, melting stops, a situation reinforced by transfer to the conductive portion of the geotherm at approximately this pressure (Chapman and Pollack, 1977).

The residual peridotite produced by this calculation has phase proportions that are close to the typical proportions given by Dick et al. (1984) for plagioclase-free abyssal peridotite (Table 3). Although this is satisfying, some circularity exists, because the original starting composition (Table 3) was constructed by combining a closely similar average of abyssal peridotites from Dick et al. (1984), Dick (1989), and Johnson et al. (1990) with a CMASN melt on the plagioclase-spinel lherzolite univariant curve at 1.1 GPa in the ratio of 80:20. However, the calculation to construct lherzolite A is not the same as the polybaric fractional melting calculation. In addition, the composition of lherzolite A (Table 3) is a close match for pyrolite and the estimated primitive mantle of Hart and Zindler (1986) and is, therefore, consistent with widespread views on the composition of the primitive mantle.

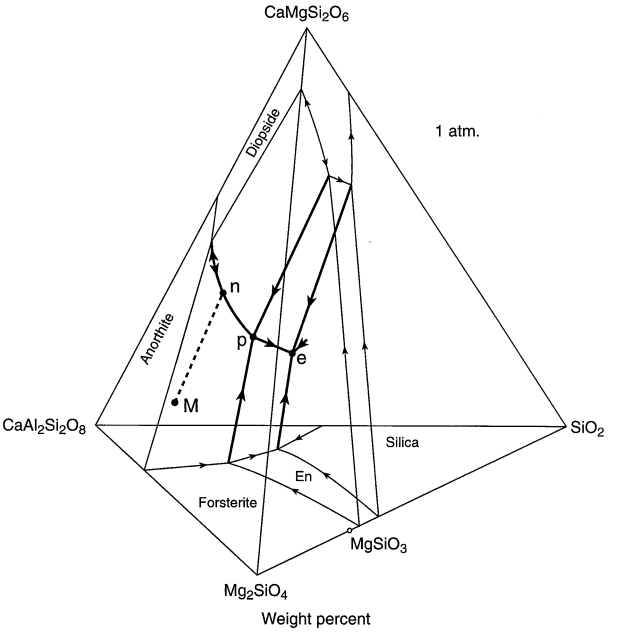

Fig. 9. Liquidus phase relations at 1 atm in the CMAS simplification of the tholeiitic basalt tetrahedron. Heavy boundary lines are within the tetrahedron, and light boundary lines are on the faces. Arrows indicate directions of decreasing temperature. The dashed line M-n lies on the anorthite-forsterite surface and is part of a liquid crystallization path. Modified from Fig. 3 of Presnall (1999) with the spinel field along the $CaAl_2Si_2O_8$-Mg_2SiO_4 edge omitted.

7. A CONSISTENCY TEST

To test the idea that the major-element characteristics of MORBs are controlled mainly by phase relations on the divariant CMASNF surface at the plagioclase-spinel lherzolite transition, we compare the fractional crystallization behavior of a representative model liquid on the divariant surface with the observed crystallization behavior of MORBs. In making this comparison, the early stages of fractional crystallization are important. The late stages of fractionation have no resolving power, because the phase relations would force convergence of liquid paths for a wide range of candidate parental magmas that may or may not be appropriate. To perform the test, we use phase relations in the CMAS tetrahedron at 1 atm (Fig. 9). To establish the validity of using the CMAS system, we show that the latter part of the liquid path indicated by phase relations in this system captures the essential features of the latter part of the liquid path for MORBs. Then we use the same phase diagram to compare the early stages of fractional crystallization of a candidate parental magma with the early stages of MORB fractionation.

The model to be tested involves the generation of melts on the CMASNF plagioclase-spinel lherzolite solidus (Fig. 8) with transport of these melts to a magma chamber in the lower part of the oceanic crust where they mix and fractionally crystallize. Alternatively, the magmas may mix and fractionally crystallize to a limited extent at intermediate pressures on their way to the shallow magma chamber (Grove et al., 1992). As a representative liquid generated on the CMASNF surface, we use point M at 1.3 GPa (Fig. 8). To describe the low-pressure fractional

crystallization behavior of M, we recast the six-component composition at M into CMAS components that leave the position of M in the Di-Pl-Ol-Q tetrahedron unchanged in the simplified Di-An-Fo-Q tetrahedron (Fig. 9). Then we calculate the crystallization path algebraically using the procedures of Presnall (1986, 1991), which are explained further in Presnall (1999). To simplify the calculation, the spinel volume that lies along the Fo-An join is omitted from Figure 9 (compare with Fig. 3 in Presnall, 1999), and the anorthite-forsterite surface is extended to the An-Fo edge of the diagram. Point M, which would have been located just inside the deleted spinel volume, now lies very slightly off the anorthite-forsterite surface in the anorthite volume. As crystallization at 1 atm of only 1% anorthite would cause the liquid path to reach the anorthite-forsterite surface and is difficult to resolve on the diagram, we start the liquid path from the point at which the liquid lies exactly on the surface after 1% crystallization of anorthite.

Figure 10 gives additional details of the crystallization history not shown in Figure 9. Compositions of diopside and enstatite used in the calculations are from Walter and Presnall (1994) and Longhi (1987). Note that the calculation indicates that 60% crystallization of olivine plus plagioclase occurs before the appearance of clinopyroxene. Figure 11b shows that for natural basalts, this percentage is an artifact of carrying out the calculation for the simplified CMAS system and should be reduced to ~40%. This is discussed further below. To reach the margin of the MORB field nearest to M, ~20% crystallization would be required. If the proportion of crystallizing plagioclase is 70% (Fig. 10), then 28% plagioclase would be crystallized at a total crystallization percentage of 40%. This is close to the maximum amount of plagioclase crystallization that can occur without producing a negative Eu anomaly (Haskin, 1984) and is consistent with the observation that more-fractionated N-MORBs show a negative Eu anomaly but less-fractionated N-MORBs do not (Saunders, 1984).

Figure 11 shows that the calculated liquid path mimics the late stages of the fractional crystallization trend of MORBs except for the slightly low olivine content of the calculated path. This is expected because of the absence of FeO from the CMAS system. The data of Presnall (1966) show that addition of FeO would shift the diopside-olivine and enstatite-olivine boundary surfaces away from quartz and toward olivine, which would move the n-p-e portion of the liquid path similarly. The experiments of Walker et al. (1979, Fig. 8) on natural oceanic basalts confirm that this shift would be just enough to bring the path into coincidence with the central region of the MORB fractionation trend. As the olivine-plagioclase surface is bounded on one side by the diopside-olivine-plagioclase univariant line, the correspondence between the CMAS and natural liquid paths during crystallization of diopside, olivine, and plagioclase indicates that the early stages of the liquid path for M along the olivine-plagioclase surface can be evaluated with similar reliability.

For this early part of the liquid path, addition of FeO to the CMAS system would reduce liquidus temperatures in the olivine volume, and addition of Na_2O would reduce liquidus temperatures in the plagioclase volume. These two effects would largely cancel each other, and the position of the olivine-plagioclase surface in the CMAS system is expected to remain relatively unchanged in the pl-ol-q projection. This has been

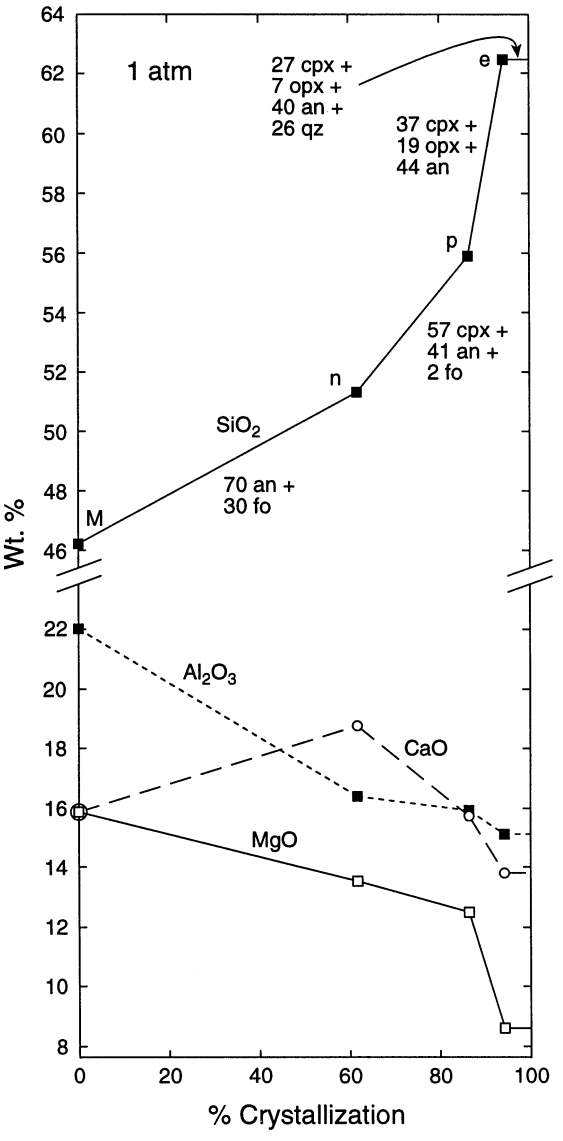

Fig. 10. Data for liquid path shown in Fig. 9. For each segment, proportions of phases crystallizing are given in wt. %. Note that point M has an MgO content of ~16%, whereas it lies on the 12% MgO contour in Fig. 8. This results from recasting the CMASNF composition as CMAS components while holding the normative proportions of Di, Pl, Ol, and Q constant. This adjustment applies also to the other oxides.

confirmed by Grove et al. (1992), but Bryan and Dick (1982) and Dick et al. (1984) have resolved small differences in MORB trends along this surface from different localities. The global MORB glass array in Figure 12 shows a slightly elongated distribution that lies directly astride the M-n path and is consistent with crystallization of plagioclase and olivine from a parental magma near M. The distribution of glass compositions on the olivine-plagioclase surface appears in Figure 6b as a widening of the MORB array at projected normative quartz proportions in the Di-Ol-Q triangle of <~40%. This widening does not occur in Figure 6a. Thus, the MORB array in three dimensions has the shape of a somewhat flattened funnel with

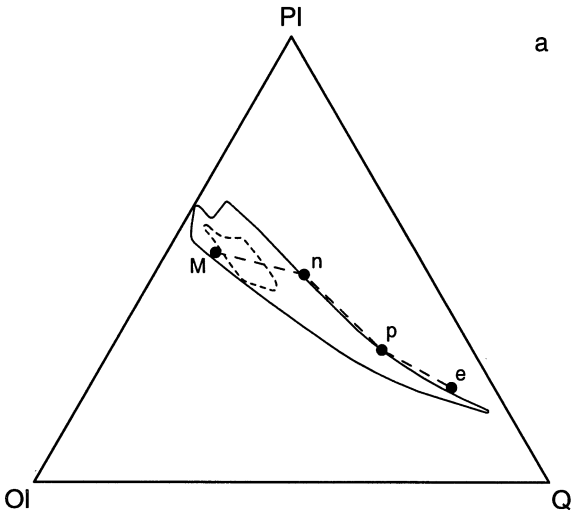

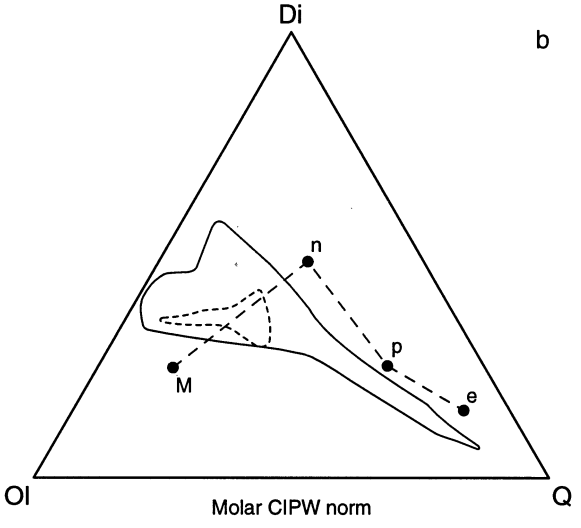

Fig. 11. Projections as in Fig. 6 of liquid path from Fig. 9 compared to the total field of MORBs (solid outline) and the most primitive MORBs (dashed outline) from Melson (1992).

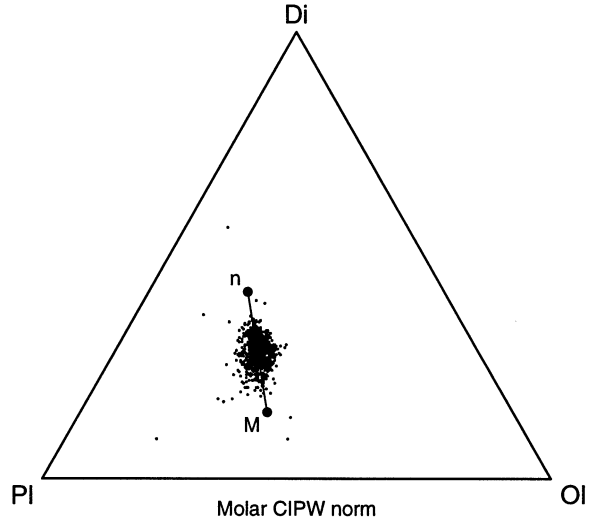

Fig. 12. Initial portion of the liquid path from Fig. 9 and MORB glass data as in Fig. 6 projected from Q onto the Di-Pl-Fo face.

the flattened portion aligned along the olivine-plagioclase surface.

Ascending melts may also fractionally crystallize at elevated pressures before they reach a crustal magma chamber. As pressure increases, the diopside volume expands while the anorthite-forsterite surface moves very little (Presnall et al., 1978). This causes the forsterite-anorthite-diopside univariant line (n-p) to move toward the anorthite-forsterite-quartz base of the tetrahedron (Fig. 9) while staying very close to the position of the anorthite-forsterite surface at 1 atm. Thus, MORB glasses lying close to the anorthite-forsterite surface, which appear consistent with crystallization controlled by olivine and plagioclase at very low pressure, could also be consistent with crystallization of these two phases plus diopside at elevated pressures. For natural compositions, Grove et al. (1992) determined how the "line" along which olivine, plagioclase, and diopside crystallize shifts with pressure up to 0.8 GPa. They showed that trends of MORBs from the Kane Fracture Zone and the MARK area south of Kane are consistent with fractionation of olivine, diopside, and plagioclase at elevated pressures, rather than just olivine and plagioclase at pressures near 1 atm. For the MORB glass array as a whole, it is difficult to determine which of these processes is dominant. Both probably contribute, and parental melts in the vicinity of M are equally consistent with either one.

Although parental magmas on the CMASNF surface in the vicinity of M are close to the primitive end of the MORB array, they lie completely outside it (Fig. 8b). For a liquid crystallization path to reach the MORB array from the region near M, crystallization of olivine alone is inadequate. Plagioclase and olivine must both crystallize. The participation of plagioclase must occur before the production of the most primitive glasses that have been observed and would be an expected phenocryst along with olivine in these most primitive lavas. A comparison of Figures 7, 8, and 9 shows that melts generated on the CMASNF solidus surface are all close to the surface along which olivine and plagioclase crystallize at 1 atm. Thus, for all these primitive melts, initial crystallization of either olivine or plagioclase would shortly be followed by crystallization of both.

To determine if the most primitive MORBs could have been derived by fractional crystallization of olivine and plagioclase from the vicinity of M, we examined phenocryst assemblages and experimental studies. Bryan and Moore (1977) provided detailed information on the phenocryst content and glass compositions of chilled pillow margins from the FAMOUS area of the Mid-Atlantic Ridge. They reported the occurrence of olivine phenocrysts with and without coexisting plagioclase phenocrysts. An interesting feature of their data (see also Hekinian et al., 1976) is that the glassy margins of the lavas containing only olivine phenocrysts have Na_2O, TiO_2, and FeO/MgO values in the same range as the lavas containing both olivine and plagioclase phenocrysts. Therefore, the lavas with plagioclase phenocrysts are not more evolved. Even though Figure 12

shows all MORB glasses, including those that are extremely fractionated, it is clear from this plot that the more primitive MORB glasses are tightly packed on the olivine-plagioclase surface, and there is no compositional trend of liquids extending toward olivine. This same observation was emphatically stated for primitive melts from the Sequeiros fracture zone (Natland, 1989). Therefore, this surface appears to be the controlling phase boundary for crystallization of even the most primitive MORBs.

A sampling of other papers giving petrographic descriptions (Muir and Tilley, 1964; Miyashiro et al., 1969; Frey et al., 1974; Shibata and Fox, 1975; Batiza et al., 1977; O'Donnell and Presnall, 1980) yields 44 MORBs with phenocrysts of both olivine and plagioclase and five with olivine alone (spinel ignored). Four of the lavas with olivine alone are from 26°N on the Mid-Atlantic Ridge (O'Donnell and Presnall, 1980) and are spatially associated with five other MORBs that contain both olivine and plagioclase phenocrysts. Again, there is no relationship between the extent of fractionation as measured by Na_2O, FeO/MgO, or TiO_2 values of the host glass and the presence or absence of plagioclase.

Experimental studies of MORBs (Bender et al., 1978; Walker et al., 1979; Grove and Bryan, 1983; Tormey et al., 1987) indicate that olivine appears before plagioclase for eight basalts studied, and plagioclase appears first for one. In all cases, the difference in temperature of appearance is $<\sim$30°C. Thus, all of these data confirm that the most primitive MORBs lie on or close to the olivine-plagioclase crystallization surface. We conclude that parental magmas with an even more primitive range of compositions near M on the CMASNF solidus surface are consistent with the petrographic and chemical features of MORBs.

8. DISCUSSION

8.1. Mantle Heterogeneity

At spreading ridges, infertile peridotite is produced as a residue of MORBs, and this peridotite is transported to subduction zones as a shallow layer overlying fertile peridotite unmodified by MORB generation. In addition, a complete range of fertile to infertile peridotite is typically found at xenolith localities that is unrelated to the enclosing basalt (e.g., Carter, 1970). Thus, widespread major element heterogeneity of mantle peridotite exists beneath continents and subduction zones, and recycling of this material back to ridges would be expected to produce MORB source regions with varying degrees of heterogeneity (Natland, 1989).

The density difference between fertile and infertile peridotite has been found to be 0.05 to 0.08 g/cm^3 (Carter, 1970; Boyd and McCallister, 1976; Jordan, 1979; Presnall and Helsley, 1982). This density difference has been shown to be more than adequate for driving the ascent of infertile peridotite plumes without any assistance from elevated temperature (Presnall and Helsley, 1982; Green et al., 2000). A homogeneous peridotite mantle would require a temperature change of approximately 400 to 600°C to achieve this amount of density change. Thus, the amount of heterogeneity observed in mantle peridotites is at least as capable a driving force for convection as temperature.

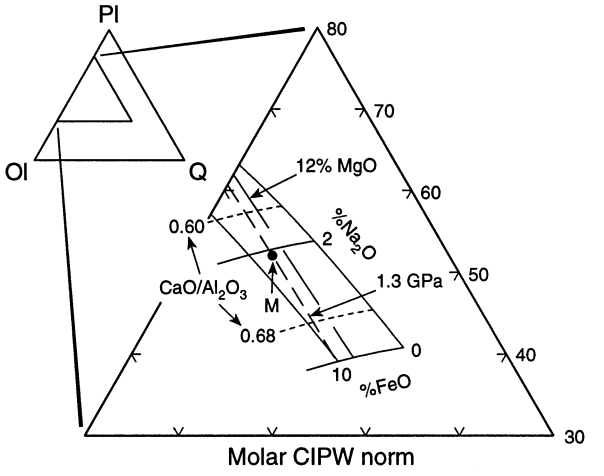

Fig. 13. CMASNF divariant surface as in Fig. 8a with added contours for MgO and CaO/Al_2O_3 in wt.%.

8.2. Generation of the Klein-Langmuir Major Element Systematics

We consider now the possibility that the form of the global inverse correlation of $(FeO)_8$ and $(CaO/Al_2O_3)_8$ with $(Na_2O)_8$ documented by Klein and Langmuir (1987, 1989) and Langmuir et al. (1992) can be produced by melting in the narrow temperature range of the plagioclase-spinel lherzolite transition interval. Because data on the compositions of liquids on the CMASNF solidus surface exist only along the Fe-free and Na-free margins, we are limited to a semiquantitative discussion of melting on this surface. Nevertheless, the existing data provide sufficient control that some general aspects of the phase relations can be discussed. Figure 13 shows that for melts generated on this surface, the contour for 12% MgO is nearly parallel to the isobar at 1.3 GPa, and as mentioned above, isotherms on this surface are nearly parallel to isobars. Melt compositions along the contour of constant MgO, which corresponds closely to constant temperature and pressure on the solidus surface, follow the form of the global trends observed by Klein and Langmuir (1987, 1989). That is, FeO and CaO/Al_2O_3 vary inversely with Na_2O. There is no topological requirement that the isobars must be parallel to contours of constant MgO and, in fact, they are not. It just happens that they are nearly parallel. Thus, for melts generated in the plagioclase-spinel lherzolite transition interval, normalization of fractionation trends to MgO = 8, as done by Klein and Langmuir (1987, 1989), is approximately equivalent to normalization to a constant pressure and temperature of generation. However, the MgO content of the basalts at their depth of origin would be $>$8%. A homogeneous mantle source would produce melts with no compositional variation at all when melted at the same temperature or when the melts are recombined after polybaric fractional melting over the same pressure range. Variation of melt compositions would require heterogeneity of the source. The nature of the heterogeneity is unimportant, because the phase relations would force conformance to the form of the $FeO\text{-}Na_2O\text{-}CaO/Al_2O_3$ systematics as long as all five crystalline phases (olivine, orthopyroxene, clinopyroxene, spinel, plagioclase) at the solidus are present.

Table 4. Primitive MORB compositions.

	Iceland[1]	Global Range[2]
SiO_2	48.72	47.2 – 51.4
TiO_2	0.93	0.50 – 1.29
Al_2O_3	15.99	15.0 – 17.58
FeO	8.96	7.21 – 8.97
MnO	0.16	0.06 – 0.21
MgO	10.56	8.39 – 10.90
CaO	14.01	11.56 – 13.35
Na_2O	1.72	1.62 – 2.49
K_2O	0.05	0.00 – 0.28

[1] Most magnesian published Icelandic glass (Breddam, 2002).
[2] 39 primitive MORB glasses from Atlantic and Pacific Oceans (Presnall and Hoover, 1987).

Although melting at ridges is probably not confined to the very narrow range of potential temperatures that would intersect the solidus in the pressure range of the plagioclase-spinel transition, we argue that melting in this pressure range exerts a dominant influence on MORB compositions globally. To the extent that this dominance exists, the need for large potential temperature variations to produce the global systematics is reduced.

8.3. Limits on the Range of Potential Temperatures at Ridges

Following Dick et al. (2002), we suggest that the near or total absence of basalts in the central region of the Gakkel Ridge indicates a cool adiabat. Chapman and Pollack (1977) calculated that the conductive portion of geotherms at ridges would intersect the volatile-free lherzolite solidus at a pressure of ~1 GPa. Therefore, no significant melt production at pressures below the stability of spinel in the CMASNF system (0.93 GPa) is expected. For this pressure limit, the T_p required for an adiabat to fall below the CO_2-free solidus and, therefore, miss basalt production, would be ~1240°C (Figures 4, 5). We take this as the approximate T_p beneath the central region of the Gakkel Ridge and a lower bound for ridges globally.

An upper bound is more difficult to establish. As pressure increases above 1.6 GPa, melts become more mafic, and the tendency to produce an olivine-controlled, low-pressure fractionation trend increases. The complete absence of picritic magmas and olivine-controlled fractionation at ridges is in sharp contrast to the situation at Hawaii, where olivine-controlled fractionation trends have been extensively documented (Wright, 1971, and referenced therein) and picritic glasses containing up to 15% MgO have been reported (Clague et al., 1991, 1995). The compositions of these picritic glasses lie along the Hawaiian trend of olivine-controlled fractionation at low pressures (Presnall, 1999). Table 4 compares the composition range of 39 primitive MORB glasses with the most magnesian published analysis of glass in Iceland, a "hot spot" similar in vigor to Hawaii. The composition of this glass is consistent with primitive MORBs from normal ridge segments with the exception of a slightly higher value for CaO. In particular, the MgO content is far less than that of picritic glasses from Hawaii. The formation of picrites is masked in some polybaric fractional melting models by mixing of high- and low-pressure melts from the melting column, but the presence of both picritic melts and olivine-controlled fractionation trends in Hawaii shows that this kind of modeling has limitations. The simplest explanation for Iceland and the Reykjanes Ridge, which lie at the highest temperature extreme of the model of Langmuir et al. (1992), is that basalt production does not extend to pressures in the range of 3 to 4 GPa where picritic melts would be produced (e.g., Gudfinnsson and Presnall, 1996). This imposes an approximate upper bound for T_p at ridges, including hot spots such as Iceland, of ~1400°C.

The T_p of 1260°C for average MORBs is only 20°C higher than the minimum for basalt production. This is an expected condition for a thermal regime dominated by the emergence of new ridges and the death of old ones. Because a shift of only 20°C in T_p causes the melt productivity to change from 0 to 24% (Table 2), emerging ridges rapidly build their melt productivity to a full crustal thickness, and fading ridges just as rapidly shut down their productivity.

8.4. Concluding Comments

The model we have proposed appears to be robust for the East Pacific Rise where MORBs are more uniform in composition (Langmuir et al., 1992), and the varying amounts of melt with depth indicated by the MELT seismic experiment (Forsyth et al., 1998, 2000) closely match the distribution expected from the phase relations and adiabat we use. The uniformity of MORB compositions along the East Pacific Rise suggests a relatively constant T_p, which is consistent with the absence of any observable variations in temperature at the 405-km discontinuity directly beneath this ridge from 40°N to 35°S (Melbourne and Helmberger, in press). As eastern Pacific MORBs lie approximately in the center of the global compositional extremes on an $(FeO)_8$ vs. $(Na_2O)_8$ plot (Klein and Langmuir, 1987), average MORBs worldwide appear also to be well modeled by melting at the plagioclase-spinel lherzolite transition.

An interesting aspect of the global systematics is that $(Na_2O)_8$ and $(FeO)_8$ are always inversely correlated, but the correlation of these oxides with axial water depth is sometimes inverted. That is, $(FeO)_8$ usually decreases with increasing water depth, but in some cases, such as the Galapagos Platform, it increases (Langmuir et al., 1992). If volcanism at these localities is produced by ascent of chemical plumes driven by their low-density, infertile compositions (Presnall and Helsley, 1982; Green et al., 2000) rather than by high temperatures, they would produce basalts low in $(FeO)_8$, and phase-equilibrium controls in the plagioclase-spinel lherzolite transition would force them to have high $(Na_2O)_8$. This would explain the inverted correlations with water depth. On the other hand, Reykjanes ridge and Icelandic basalts, which lie at the high T_p end of the "normal" correlation showing increasing $(FeO)_8$ with decreasing water depth, may be a case where an elevated T_p is more important than heterogeneity. A completely satisfactory explanation for Iceland remains elusive. The complete absence of picritic glasses at Iceland argues against strongly elevated temperatures, and the preliminary seismic evidence for a deep low-velocity column beneath Iceland (Wolfe et al., 1997) was shown to be unclear (Keller et al., 2000). Subsequently, a more comprehensive seismic study (Foulger et al.,

2001) resolved a cylindrical low wave-speed body in the upper 250 km that changes at greater depths to a flattened column with a north-south elongation. The global ridge system and its associated hot spots may represent a complex mix of temperature variations and mantle heterogeneity. An understanding of this issue would have the additional benefit of helping to clarify the roles of temperature and heterogeneity in mantle dynamics generally.

Acknowledgments—We are especially pleased to participate in this volume in honor of Hat Yoder, whose early studies laid the framework for subsequent experimental studies on basalt petrogenesis. We thank Hat Yoder, Tony Morse, and the journal reviewers, Tim Grove and Paul Asimow, for penetrating and sometimes withering reviews that led to significant improvements in the manuscript. The assistance of Paul Asimow in developing the comparison of our experimental data with MELTS is especially appreciated. Don Forsyth generously provided an unpublished tomographic image from the MELT experiment and very helpful comments about its interpretation. Presnall thanks Don Anderson for stimulating conversations that helped clarify some of the issues discussed. Financial support was provided by National Science Foundation Grants EAR-9725900 and EAR-0106645 to Presnall. Contribution No. 943, Department of Geosciences, University of Texas at Dallas.

Associate editor: F. A. Frey

REFERENCES

Allègre C. J., Pineauz F., Bernat M., and Javoy M (1971) Evidence for the occurrence of carbonatites on the Cape Verde and Canary Islands. *Nature* **233,** 102–103.

Anderson D. L. and Sammis C. (1970) Partial melting in the upper mantle. *Phys. Earth Planet. Int.* **3,** 41–50.

Asimow P. D., Hirschmann M. M., Ghiorso M. S., O'Hara M. J., and Stolper E. M. (1995) The effect of pressure-induced solid-solid phase transitions on decompression melting of the mantle. *Geochim. Cosmochim. Acta* **59,** 4489–4506.

Asimow P. D., Hirschmann M. M., and Stolper E. M. (2001) Calibration of peridotite partial melting from thermodynamic models of minerals and melts, IV. Adiabatic decompression and the composition and mean properties of mid-ocean ridge basalts. *J. Petrol.* **42,** 963–998.

Baker M. B., Hirschmann M. M., Ghiorso M. S., and Stolper E. M. (1995) Compositions of near-solidus peridotite melts from experiments and thermodynamic calculations. *Nature* **375,** 308–311.

Baker M. B., Hirschmann M. M., Wasylenki L. E., Stolper E. M., and Ghiorso M. S. (1996) Quest for low-degree mantle melts: Reply. *Nature* **381,** 286.

Batiza R., Rosendahl B. R., and Fisher R. L. (1977) Evolution of oceanic crust 3. Petrology and geochemistry of basalts from the East Pacific Rise and the Siqueiros transform fault. *J. Geophys. Res.* **82,** 265–276.

Bell D. R. and Rossman G. R. (1992) Water in Earth's mantle: The role of nominally anhydrous minerals. *Science* **255,** 1391–1397.

Bender J. F., Hodges F. N., and Bence A. E. (1978) Petrogenesis of basalts from the project FAMOUS area: Experimental study from 0 to 15 kbars. *Earth Planet. Sci. Lett.* **41,** 277–302.

Breddam K. (2002) Kistufell: Primitive melt from the Iceland mantle plume. *J. Petrol.* **43,** 345–373.

Bryan W. B. and Moore J. G. (1977) Compositional variations of young basalts in the Mid-Atlantic Ridge rift valley near lat. 36°49'N. *Geol. Soc. Am. Bull.* **88,** 556–570.

Bryan W. B. and Dick H. J. B. (1982) Contrasted abyssal basalt liquidus trends: Evidence for mantle major element heterogeneity. *Earth Planet. Sci. Lett.* **58,** 15–26.

Bryan W. B., Thompson G., Frey F. A., and Dickey J. S. (1976) Inferred geologic settings and differentiation in basalts from the Deep-Sea Drilling Project. *J. Geophys. Res.* **81,** 4285–4304.

Byers C. D., Christie D. M., Muenow D. W., and Sinton J. M. (1984) Volatile contents and ferric ferrous ratios of basalt, ferrobasalt, andesite and rhyodacite glasses from the Galapagos 95.5° W propagating rift. *Geochim. Cosmochim. Acta* **48,** 2239–2245.

Byers C. D., Garcia M. O., and Muenow D. W. (1986) Volatiles in basaltic glasses from the East Pacific Rise at 21° N: Implications for MORB sources and submarine lava flow morphology. *Earth Planet. Sci. Lett.* **79,** 9–20.

Boyd F. R. and McCallister R. H. (1976) Densities of fertile and sterile garnet peridotites. *Geophys. Res. Lett.* **3,** 509–512.

Carter J. L. (1970) Mineralogy and chemistry of the Earth's upper mantle based on the partial fusion-partial crystallization model. *Geol. Soc. Am.* **81,** 2021–2034.

Chapman D. S. and Pollack H. N. (1977) Regional geotherms and lithospheric thickness. *Geology* **5,** 265–268.

Clague D. A., Weber W., and Dixon J. E. (1991) Picritic glasses from Hawaii. *Nature* **353,** 553–556.

Clague D. A., Moore J. G., Dixon J. E., and Friesen W. B. (1995) Petrology of submarine lavas from Kilauea's Puna Ridge, Hawaii. *J. Petrol.* **36,** 299–349.

Dalton J. A. and Presnall D. C. (1998a) Carbonatitic melts along the solidus of model lherzolite in the system CaO-MgO-Al_2O_3-SiO_2-CO_2 from 3 to 7 GPa. *Contrib. Mineral. Petrol.* **131,** 123–135.

Dalton J. A. and Presnall D. C. (1998b) The continuum of primary carbonatitic-kimberlitic melt compositions in equilibrium with lherzolite: Data from the system CaO-MgO-Al_2O_3-SiO_2-CO_2 at 6 GPa. *J. Petrol.* **39,** 1953–1964.

Davis B. T. C. and Schairer F. (1965) Melting relations in the join diopside-forsterite-pyrope at 40 kilobars and at one atmosphere. *Carnegie Inst. Wash. Year Book* **64,** 123–126.

Dick H. J. B. (1989) Abyssal peridotites, very slow spreading ridges and ocean ridge magmatism. In *Magmatism in the Ocean Basins* (eds. A. D. Saunders and M. J. Norry), pp. 71–105, *Geol. Soc. Spec. Pub. 42*.

Dick H. J. B., Fisher R. L., and Bryan W. B. (1984) Mineralogic variability of the uppermost mantle along mid-ocean ridges. *Earth Planet. Sci. Lett.* **69,** 88–106.

Dick H. J. B., Kurras G. J., Snow J., Jokat W., Michael P., and Langmuir C. (2002) Volcanic and tectonic processes along the Gakkel Ridge; Morphologic interpretation of axial valley features and samples from the Arctic Mid-Ocean Ridge Expedition (AMORE 2001). *EOS Trans. Am. Geophys. Union* **82,** F1098.

Dixon J. E. and Clague D. A. (2001) Volatiles in basaltic glasses from Loihi Seamount, Hawaii: Evidence for a relatively dry plume component. *J. Petrol.* **42,** 627–654.

Dixon J. E., Stolper E., and Delaney J. R. (1988) Infrared spectroscopic measurements of CO_2 and H_2O in Juan de Fuca Ridge basaltic glasses. *Earth Planet. Sci. Lett.* **90,** 87–104.

Donaldson C. H. and Brown R. W. (1977) Refractory megacrysts and magnesium-rich melt inclusions within spinel in oceanic tholeiites: Indicators of magma mixing and parental magma composition. *Earth Planet. Sci. Lett.* **37,** 81–89.

Dunn R. and Forsyth D. (2001) Short-period Love waves reveal the transition from broad mantle upwelling to the narrow crustal magmatic system beneath the southern East Pacific Rise. *EOS Trans. Am. Geophys. Union* **82,** F1113.

Dziewonski A. M. and Anderson D. L. (1981) Preliminary reference Earth model. *Phys. Earth Planet. In.* **25,** 297–356.

Eggler D. H. (1975) Peridotite-carbonate relations in the system CaO-MgO-SiO_2-CO_2. *Carnegie Inst. Wash. Year Book* **74,** 468–474.

Eggler D. H. (1976) Does CO_2 cause partial melting in the low-velocity layer of the mantle? *Geology* **4,** 69–72.

Eggler D. H. (1978) The effect of CO_2 upon partial melting of peridotite in the system Na_2O-CaO-Al_2O_3-MgO-SiO_2-CO_2 to 35 kb, with an analysis of melting in a peridotite-H_2O-CO_2 system. *Am. J. Sci.* **278,** 305–343.

Ekstrom G. (2000) Mapping the lithosphere and asthenosphere with surface waves: Lateral structure and anisotropy. In *The History and Dynamics of Global Plate Motions* (eds. M. A. Richards, et al), pp. 239–255, *Geophys. Mon. 121, Am. Geophys. Union*.

Engel A. E. J. and Engel C. G. (1964a) Composition of basalts from the Mid-Atlantic Ridge. *Science* **144,** 1330–1333.

Engel A. E. J. and Engel C. G. (1964b) Igneous rocks of the East Pacific Rise. *Science* **146,** 477–485.

Engel A. E. J., Engel C. G., and Havens R. G. (1965) Chemical characteristics of oceanic basalts and the upper mantle. *Geol. Soc. Am. Bull.* **76,** 719–734.

Falloon, T. J. and Green, D. H. (1988) Anhydrous partial melting of peridotite from 8 to 35 kb and the petrogenesis of MORB. *J. Petrol.* **Spec. Lithospheric Issue,** 374–414.

Falloon, T. J. and Green, D. H. (1989) The solidus of carbonated, fertile peridotite. *Earth Planet. Sci. Lett.* **94,** 364–370.

Falloon T. J., Green D. H., Hatton C. J., and Harris K. L. (1988) Anhydrous partial melting of a fertile and depleted peridotite from 2 to 30 kb and application to basalt petrogenesis. *J. Petrol.* **29,** 1257–1282.

Falloon T. J., Green D. H., O'Neill H. St. C., and Ballhaus C. G. (1996) Quest for low-degree mantle melts. *Nature* **381,** 285.

Faul U. H. (2001) Melt retention and segregation beneath mid-ocean ridges. *Nature* **410,** 920–923.

Foulger G. R., Pritchard M. J., Julian B. R., Evans J. R., Allen R. M., Noelt G., Morgan W. J., Bergsson B. H., Erlendsson P., Jakobsdottir S., Ragnarsson S., Stefansson R., and Vogfjörd K. (2001) Seismic tomography shows that upwelling beneath Iceland is confined to the upper mantle. *Geophys. J. Int.* **146,** 504–530.

Forsyth D. W., Webb S., Dorman L. M., and Shen Y. (1998) Phase velocities of Rayleigh waves in the MELT experiment on the East Pacific Rise. *Science* **280,** 1235–1238.

Forsyth, D. W., Webb, S., Dorman, L. M., and Shen, Y. (2000) Three-dimensional mantle structure beneath the East Pacific Rise in the MELT area from Rayleigh wave dispersion. In *Second RIDGE Workshop on Mantle Flow and Melt Generation beneath Mid-Ocean Ridges: Constraints from MELT and Other Experiments and Observations.* p. 5, RIDGE Office, Corvallis, OR.

Frey F. A., Bryan W. B., and Thompson G. (1974) Atlantic Ocean floor: Geochemistry and petrology of basalts from legs 2 and 3 of the Deep-Sea Drilling Project. *J. Geophys. Res.* **79,** 5507–5527.

Gaboret C., Forte A. M., and Montagner J-P. (2000) Comparison of the predictions of convection-induced mantle deformations with the seismic anisotropy. *EOS T. Am. Geophys. Un.* **81,** F1240.

Galer S. J. G. and O'Nions R. K. (1986) Magmagenesis and the mapping of chemical and isotopic variations in the mantle. *Chem. Geol.* **56,** 45–61.

Gasparik T. (1984) Two-pyroxene thermobarometry with new experimental data in the system CaO-MgO-Al_2O_3-SiO_2. *Contrib. Mineral. Petrol.* **87,** 87–97.

Gerlach T. M. and Graeber E. J. (1985) Volatile budget of Kilauea Volcano. *Nature* **313,** 273–277.

Gerlach T. M., McGee K. A., Tamar E., Sutton A. J., and Doukas M. P. (2001) CO_2 degassing at Kilauea Volcano. Implications for primary magma, summit reservoir dynamics, and magma supply monitoring. *EOS Trans. Am. Geophys. Union* **82,** F1327.

Ghiorso M. S. and Sack R. O. (1995) Chemical mass transfer in magmatic processes; IV. A revised and internally consistent thermodynamic model for the interpolation and extrapolation of liquid-solid equilibria in magmatic systems at elevated temperatures and pressures. *Contrib. Mineral. Petrol.* **119,** 197–212.

Ghiorso, M. S., Hirschmann, M. M., Reiners, P., and Kress, V. C. III (submitted) pMELTS: A revision of MELTS for improved calculation of phase relations and major element partitioning related to partial melting of the mantle to 3 GPa. *Geochem. Geophys. Geosys*.

Green D. H., Falloon T. J., Eggins S. M., and Yaxley G. M. (2000) Primary magmas and mantle temperatures. *Eur. J. Mineral.* **13,** 437–451.

Grove T. L. and Bryan W. B. (1983) Fractionation of pyroxene-phyric MORB at low pressure: An experimental study. *Contrib. Mineral. Petrol.* **84,** 298–309.

Grove T. L., Kinzler R. J., and Bryan W. B. (1992) Fractionation of mid-ocean ridge basalt (MORB). In *Mantle Flow and Melt Generation at Mid-Ocean Ridges* (eds. J. Phipps Morgan, D. K. Blackman, J. M. Sinton), pp. 281–310, *Geophys. Mon. 71, Am. Geophys. Union*.

Gudfinnsson G. H. and Presnall D. C. (1996) Melting relations of model lherzolite in the system CaO-MgO-Al_2O_3-SiO_2 at 2.4– 3.4 GPa and the generation of komatiites. *J. Geophys. Res.* **101,** 27701–27709.

Gudfinnsson G. H. and Presnall D. C. (2000) Melting behavior of model lherzolite in the system CaO-MgO-Al_2O_3-SiO_2-FeO at 0.7 to 2.8 GPa. *J. Petrol.* **41,** 1241–1269.

Hart S. R. and Zindler A. (1986) In search of a bulk-earth composition. *Chem. Geol.* **57,** 247–267.

Haskin L. A. (1984) Petrogenetic modelling—Use of rare earth elements. *Rare Earth Element Geochemistry* (ed. P. Henderson), 115–152. Elsevier.

Hauri E. H., Shimizu N., Dieu J. J., and Hart S. R. (1993) Evidence for hotspot-related carbonatite metasomatism in the oceanic upper mantle. *Nature* **365,** 221–227.

Hekinian R., Moore J. G., and Bryan W. B. (1976) Volcanic rocks and processes of the Mid-Atlantic Ridge rift valley near 36°49'N. *Contrib. Mineral. Petrol.* **58,** 83–110.

Herzberg, C. and O'Hara, M. J. (1972) Temperature and pressure calibration and reproducibility of pressure in solid media equipment. *Progress in Experimental Petrology*. Nat. Environment Res. Council Pub. Ser. D, No. **2,** 97–98.

Hirschmann, M. M. (2000) Mantle solidus. Experimental constraints and the effects of peridotite composition. *Geochem. Geophys. Geosys. 1(article)*:2000GC000070.

Hirschmann M. M., Baker M. B., and Stolper E. M. (1998) The effect of alkalis on the silica content of mantle-derived melts. *Geochim. Cosmochim. Acta* **62,** 883–902.

Jaques A. L. and Green D. H. (1980) Anhydrous melting of peridotite at 0–15 kb pressure and the genesis of tholeiitic basalts. *Contrib. Mineral. Petrol.* **73,** 287–310.

Johnson K. T. M., Dick H. J. B., and Shimizu N. (1990) Melting in the oceanic upper mantle: An ion microprobe study of diopsides in abyssal peridotites. *J. Geophys. Res.* **95,** 2661–2678.

Jordan T. H. (1979) Mineralogies, densities and seismic velocities of garnet lherzolites and their geophysical implications: Inclusions in Kimberlites and other Volcanics. In *The Mantle Sample* (eds. F. R. Boyd and H. O. A. Meyer), pp. 1–14, *Proc. 2nd Int. Kimberlite Conf., Vol. 2, Am. Geophys. Union*.

Kelemen P., Hirth G., Shimizu N., Spiegelman M., and Dick H. J. B. (1997) A review of melt migration processes in the adiabatically upwelling mantle beneath oceanic spreading ridges. *Phil. Trans. R. Soc. Lond. A.* **355,** 283–318.

Keller W. R., Anderson D. L., and Clayton R. W. (2000) Resolution of tomographic models of the mantle beneath Iceland. *Geophys. Res. Lett.* **27,** 3993–3996.

Kinzler R. J. and Grove T. L. (1992a) Primary magmas of mid-ocean ridge basalts, 2. Application. *J. Geophys. Res.* **97,** 6907–6926.

Kinzler R. J. and Grove T. L. (1992b) Primary magmas of mid-ocean ridge basalts, 1. Experiments and methods. *J. Geophys. Res.* **97,** 6885–6906.

Klein E. M. and Langmuir C. H. (1987) Global correlations of ocean ridge basalt chemistry with axial depth and crustal thickness. *J. Geophys. Res.* **92,** 8089–8115.

Klein E. M. and Langmuir C. H. (1989) Local versus global variations in ocean ridge basalt composition: A reply. *J. Geophys. Res.* **94,** 4241–4252.

Kogarko L. N. (1993) Geochemical characteristics of oceanic carbonatites from the Cape Verde Islands. *S. Afr. J. Geol.* **96,** 119–125.

Kohlstedt D. L., Keppler H., and Rubie D. C. (1996) Solubility of water in theα,β, andγ phases of $(Mg, Fe)_2SiO_4$. *Contrib. Mineral. Petrol.* **123,** 345–357.

Kohn S. C. (1996) Solubility of H_2O in nominally anhydrous mantle minerals using ^1H MAS NMR. *Am. Mineral.* **81,** 1523–1526.

Kushiro I. (1973) Origin of some magmas in oceanic and circumoceanic regions. *Tectonophysics* **17,** 211–222.

Kushiro I. (2001) Partial melting experiments on peridotite and origin of mid-ocean ridge basalts. *Ann. Rev. Earth Planet. Sci.* **29,** 71–107.

Kushiro I. and Yoder Jr. H. S. (1966) Anorthite-forsterite and anorthite-enstatite reactions and their bearing on the basalt-eclogite transformation. *J. Petrol.* **7,** 337–362.

Lambert I. B. and Wyllie P. J. (1968) Stability of hornblende and a model for the low velocity zone. *Nature* **219,** 1240–1241.

Langmuir C. H., Klein E. M., and Plank T. (1992) Petrological systematics of mid-ocean ridge basalts: Constraints on melt generation beneath ocean ridges. In *Mantle Flow and Melt Generation at*

Mid-Ocean Ridges (eds. J. Phipps Morgan, D. K. Blackman and J. M. Sinton), pp. 183–280, *Geophys. Mon. 71, Am. Geophys. Union*.

Le Bas M. J. (1984) Oceanic Carbonatites: Kimberlites and Related Rocks. *Kimberlites I* (ed. J. Kornprobst), 169–178. Elsevier.

Longhi J. (1987) Liquidus equilibria and solid solution in the system $CaAl_2Si_2O_8$-Mg_2SiO_4-$CaSiO_3$-SiO_2 at low pressure. *Am. J. Sci.* **287,** 265–331.

Matveev S., O'Neill H. St. C., Ballhaus C., Taylor W. R., and Green D. H. (2001) Effect of silica activity on OH^- IR spectra of olivine: Implications for low-*a*SiO_2 mantle metasomatism. *J. Petrol.* **42,** 721–729.

McKenzie D. (1985) The extraction of magma from the crust and mantle. *Earth Planet. Sci. Lett.* **74,** 81–91.

McKenzie D. and Bickle M. J. (1988) The volume and composition of melt generated by extension of the lithosphere. *J. Petrol.* **29,** 625–697.

Melbourne, T., and Helmberger, D. V. (in press) Precise transition zone thickness estimates from triplicated multiple S. *J. Geophys. Res*.

Melson, W. G. (1992) *VGGP Database of Basalt Glass Analyses.* Smithsonian Institution, Washington, D. C.

MELT Seismic Team (1998) Imaging the deep seismic structure beneath a mid-ocean ridge: The MELT experiment. *Science* **280,** 1215–1218.

Michael P. J. (1988) The concentration, behavior and storage of H_2O in the suboceanic upper mantle: Implications for mantle metasomatism. *Geochim. Cosmochim. Acta* **52,** 555–566.

Michael P. J. (1995) Regionally distinctive sources of depleted MORB: Evidence from trace elements and H_2O. *Earth Planet. Sci. Lett.* **131,** 301–320.

Minarik W. G. and Watson E. B. (1995) Interconnectivity of carbonate melt at low melt fraction. *Earth Planet. Sci. Lett.* **133,** 423–437.

Miyashiro A., Shido F., and Ewing M. (1969) Diversity and origin of abyssal tholeiite from the Mid-Atlantic Ridge near 24° and 30° North latitude. *Contrib. Mineral. Petrol.* **23,** 38–52.

Moore J. G., Batchelder J. N., and Cunningham C. G. (1977) CO_2-filled vesicles in mid-ocean basalt. *J. Volcanol. Geoth. Res.* **2,** 309–349.

Muir I. D. and Tilley C. E. (1964) Basalts from the northern part of the rift zone of the Mid-Atlantic Ridge. *J. Petrol.* **5,** 409–434.

Natland J. H. (1989) Partial melting of a lithologically heterogeneous mantle: Inferences from crystallization histories of magnesian abyssal tholeiites from the Sequieros fracture zone. In *Magmatism in the Ocean Basins* (eds. A. D. Saunders and M. J. Norry), pp. 41–70, *Geol. Soc. Spec. Pub. 42*.

Nishimura C. E. and Forsyth D. W. (1989) The anisotropic structure of the upper mantle in the Pacific. *Geophys. J.* **96,** 203–229.

O'Donnell, T. H., and Presnall, D. C. (1980) Chemical variations of the glass and mineral phases in basalts dredged from 25°–30° N along the Mid-Atlantic Ridge. *Am. J. Sci.* **Jackson Vol. 280-A,** 845–868.

O'Hara M. J. (1968) Are ocean floor basalts primary magma? *Nature* **220,** 683–686.

O'Hara M. J., Richardson S. W., and Wilson G. (1971) Garnet-peridotite stability and occurrence in crust and mantle. *Contrib. Mineral. Petrol.* **32,** 48–68.

Plank T. and Langmuir C. H. (1992) Effects of the melting regime on the composition of the oceanic crust. *J. Geophys. Res.* **97,** 19749–19770.

Presnall D. C. (1966) The join forsterite-diopside-iron oxide and its bearing on the crystallization of basaltic and ultramafic magmas. *Am. J. Sci.* **264,** 753–809.

Presnall D. C. (1976) Alumina content of enstatite as a geobarometer for plagioclase and spinel lherzolites. *Am. Mineral.* **61,** 582–588.

Presnall D. C. (1980) A double partial melt zone in the mantle beneath mid-ocean ridges. *Phys. Earth Planet. Int.* **23,** 103–111.

Presnall D. C. (1986) An algebraic method for determining equilibrium crystallization and fusion paths in multicomponent systems. *Am. Mineral.* **71,** 1061–1070.

Presnall D. C. (1991) Algebraic methods for determining directions of decreasing temperature along isobaric liquidus univariant lines. *Can. Mineral.* **29,** 687–692.

Presnall D. C. (1999) Effect of pressure on the fractional crystallization of basaltic magma. In *Mantle Petrology: Field Observations and High Pressure Experimentation: A Tribute to Francis R. (Joe) Boyd*. (eds. Y. Fei, C. M. Bertka, and B. O. Mysen), pp. 209–224, Geochem. Soc. Spec. Pub. 6.

Presnall D. C. and Helsley C. E. (1982) Diapirism of depleted peridotite—A model for the origin of hot spots. *Phys. Earth Planet. Int.* **29,** 148–160.

Presnall D. C. and Hoover J. D. (1984) Composition and depth of origin of primary mid-ocean ridge basalts. *Contrib. Mineral. Petrol.* **87,** 170–178.

Presnall D. C. and Hoover J. D. (1987) High pressure phase equilibrium constraints on the origin of mid-ocean ridge basalts. In *Magmatic Processes: Physicochemical Principles* (ed. B. O. Mysen). pp. 75–89, Geochem. Soc. Spec. Pub. 1.

Presnall D. C., Dixon S. A., Dixon J. R., O'Donnell T. H., Brenner N. L., Schrock R. L., and Dycus D. W. (1978) Liquidus phase relations on the join diopside-forsterite-anorthite from 1 atm to 20 kbar: Their bearing on the generation and crystallization of basaltic magma. *Contrib. Mineral. Petrol.* **66,** 203–220.

Presnall D. C., Dixon J. R., O'Donnell T. H., and Dixon S. A. (1979) Generation of mid-ocean ridge tholeiites. *J. Petrol.* **20,** 3–35.

Richardson C. and McKenzie D. (1994) Radioactive disequilibria from 2D models of melt generation by plumes and ridges. *Earth Planet. Sci. Lett.* **128,** 425–437.

Ringwood A. E. (1975) *Composition and Petrology of the Earth Mantle*. McGraw Hill.

Roedder E. (1965) Liquid CO_2 inclusions in olivine-bearing nodules and phenocrysts from basalts. *Am. Mineral.* **50,** 1746–1782.

Roedder E. (1984) *Fluid inclusions*. *Min. Soc. Am. Rev. Mineral.* **12,** 644 p.

Saunders A. D. (1984) The rare earth element characteristics of igneous rocks from the ocean basins. *Rare Earth Element Geochemistry* (ed. P. Henderson), 205–236. Elsevier.

Shibata T. and Fox P. J. (1975) Fractionation of abyssal tholeiites: Samples from the Oceanographer Fracture Zone (35° N, 35° W). *Earth Planet. Sci. Lett.* **27,** 62–72.

Silva L. C., Le Bas M. J., and Robertson A. H. F. (1981) An oceanic carbonatite volcano on Santiago, Cape Verde Islands. *Nature* **294,** 644–645.

Stakes D. S., Shervais J. W., and Hopson C. A. (1984) The volcanic-tectonic cycle of the FAMOUS and AMAR valleys, Mid-Atlantic Ridge (36°47'N): Evidence from basalt glass and phenocryst compositional variations for a steady state magma chamber beneath the valley mid-sections, AMAR 3. *J. Geophys. Res.* **89,** 6995–7028.

Takahashi, E., and Kushiro, I. (1983) Melting of a dry peridotite at high pressures and basalt magma genesis. *Am. Mineral.* **68,** 859–879.

Toomey D. R., Wilcock W. S. D., Solomon S. C., Hammond W. C., and Orcutt J. A. (1998) Mantle seismic structure beneath the MELT region of the East Pacific Rise from P and S wave tomography. *Science* **280,** 1224–1227.

Toomey, D. R., Conder, J. A., Wilcock, W. S. D., Forsyth, D. W., Blundy, J., Parmentier, E. M., and Hammond W. C. (submitted) Mantle dynamics in the MELT region of the East Pacific Rise. *Earth Planet. Sci. Lett.*.

Tormey R., Grove T. L., and Bryan W. B. (1987) Experimental petrology of normal MORB near the Kane Fracture Zone: 22°–25° N, Mid-Atlantic Ridge. *Contrib. Mineral. Petrol.* **96,** 121–139.

Walker D., Shibata T., and DeLong E. (1979) Abyssal tholeiites from the Oceanographer Fracture Zone. *Contrib. Mineral. Petrol.* **70,** 111–125.

Walter M. J. (1998) Melting of garnet peridotite and the origin of komatiite and depleted lithosphere. *J. Petrol.* **39,** 26–60.

Walter M. J. and Presnall D. C. (1994) Melting behavior of simplified lherzolite in the system CaO-MgO-Al_2O_3-SiO_2-Na_2O from 7 to 35 kbar. *J. Petrol.* **35,** 329–359.

Wendlandt R. F. and Mysen B. O. (1980) Melting phase relations of natural peridotite + CO_2 as a function of degree of partial melting at 15 and 30 kbar. *Am. Mineral.* **65,** 37–44.

Weng, Y-H. (1997) Liquidus phase relations for the model basaltic tetrahedron diopside-anorthite-forsterite-quartz in the system CaO-MgO-Al_2O_3-SiO_2 at 5 GPa. Ph.D. dissertation, University of Texas at Dallas.

Withers A. C., Wood B. J., and Carroll M. R. (1998) The OH component of pyrope at high pressure. *Chem. Geol.* **147,** 161–171.

Wolfe C. J., Bjarnason I. T., VanDecar J. C., and Solomon S. C. (1997) Seismic structure of the Iceland Mantle plume. *Nature* **385,** 245–247.
Wright, T. L. (1971) Chemistry of Kilauea and Mauna Loa lavas in space and time. *U. S. Geol. Survey Prof. Paper* **735,** 40 pp.
Wyllie P. J. (1977) Mantle fluid compositions buffered by carbonates in peridotite-CO_2-H_2O. *J. Geol.* **85,** 187–207.
Wyllie P. J. and Huang W. L. (1975) Peridotite, kimberlite and carbonatite explained in the system CaO-MgO-SiO_2-CO_2. *Geology* **3,** 621–624.
Wyllie P. J. and Huang W. L. (1976) Carbonation and melting reactions in the system CaO-MgO-SiO_2-CO_2 at mantle pressures with geophysical and petrological applications. *Contrib. Mineral. Petrol.* **54,** 79–107.
Yang N.-J., Sen G., and Shimizu N. (1998) Mid-ocean ridge melting: Constraints from lithospheric xenoliths at Oahu, Hawaii. *J. Petrol.* **39,** 277–295.
Zhang Y. and Zindler A. (1993) Distribution and evolution of carbon and nitrogen in Earth. *Earth Planet. Sci. Int.* **117,** 331–345.

APPENDIX

Large discrepancies exist between phase relations determined experimentally (Walter and Presnall, 1994; Gudfinnsson and Presnall, 2000) and those calculated from MELTS (Ghiorso and Sack, 1995) and pMELTS (M. S. Ghiorso et al., submitted). Figure 14 shows our CMASN solidus in the region of the plagioclase-spinel lherzolite transition and two calculated solidus curves generously provided by P. Asimow (pers. comm.), one calculated from MELTS and the other from pMELTS. To provide a direct comparison free of uncertainties due to additional components not present in the CMASNF system, both of the calculated curves are for CMASNF peridotite in equilibrium with Fe that contains 0.001% TiO_2, 0.001% Fe_2O_3, and 0.0001% K_2O to stabilize the calculation. No Cr_2O_3 is present. The bulk composition is 44.6% SiO_2, 6.19% Al_2O_3, 7.418% FeO, 37.44% MgO, 4.06% CaO, and 0.29% Na_2O (cf. Table 3). The P-T position of the curve defining the CMASN solidus in the plagioclase-spinel lherzolite transition interval is experimentally indistinguishable from that of the CMASF solidus determined in equilibrium with Fe, and we have assumed that the CMASNF solidus also lies essentially along the same line in P-T space.

The MELTS curve is essentially the same as the curve shown in Asimow et al. (2001) but raised ~35°C because of the absence of minor components. In comparison to the experimentally determined curve, note the lower temperatures and the much lower pressure range for the plagioclase-spinel lherzolite transition in the calculated curves. In addition, the calculated curves have a negative slope in the region of the plagioclase-spinel lherzolite transition, whereas the experimentally determined curve has a positive slope. The differences in slope are significant for this paper because the calculated curves require crystallization on isentropic decompression, but the experimentally determined curve requires melting.

At 1 atm, the lherzolite solidus in the CMAS system has been tightly bracketed at 1241°C by two runs of 48 and 72 h (Presnall et al., 1979). The solidus at one atm calculated from MELTS is ~1280°C but must be <1241°C because of the presence of FeO and Na_2O. Both of these components would lower the temperature. The solidus temperature calculated from pMELTS is ~1230°C, which is consistent with the CMAS result, but even this temperature may be slightly high.

The univariant curve that defines the CMASN solidus slope is constrained by a large number of runs in the CMAS system at the Na_2O-free end (Walter and Presnall, 1994; Presnall, 1976), which provides a secure starting point at 0.93 GPa for extension of the curve into CMASN space. Its positive slope and slight upward curvature are defined by the intersection of two parameterized curved surfaces, one at higher temperatures for the assemblage fo + opx + cpx + sp + liq and the other at lower temperatures for the assemblage fo + opx + cpx + pl + liq. The lower-temperature surface is based on 10 runs and the upper on five runs, in addition to the separately determined bounding curves for the CMAS system (Walter and Presnall, 1994; Presnall, 1976). This procedure for determining the position of the curve is different from the procedure initially used by Walter and Presnall (1994) and gives a slightly but not significantly different location. The corresponding curve in CMASF space is defined by its starting point in the CMAS system, one run at 1.2 GPa directly on the curve and two runs at 1.1 GPa that closely bracket the curve between 1310 and 1320°C (Gudfinnsson and Presnall, 2000). Thus, although a total description of the CMASNF surface adequate to support detailed compositional modeling of MORB petrogenesis is lacking, we believe that the boundaries and P-T slope of the surface are well-defined by the existing data.

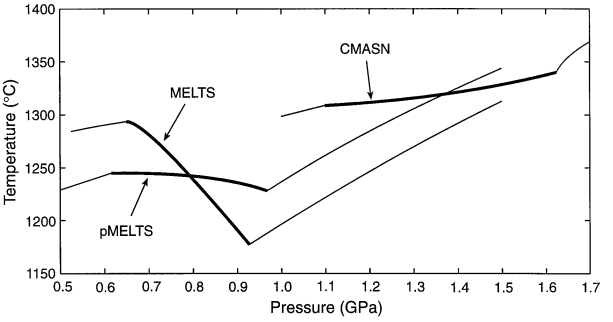

Fig. 14. Comparison of solidus curves in the CMASNF system. The experimental curve for the CMASN system (Walter and Presnall, 1994) is defined in the plagioclase-spinel lherzolite transition interval by a univariant curve that is experimentally indistinguishable in P-T space from a similar curve in the CMASF system (Gudfinnsson and Presnall, 2000). The MELTS and pMELTS curves were calculated by P. Asimow (pers. comm.) from Ghiorso and Sack (1995) and M. S. Ghiorso et al. (submitted). Heavy lines indicate the range of the plagioclase-spinel lherzolite transition for each curve.

This comparison shows that most of the differences between the model system data and phase relations calculated by MELTS and pMELTS for more complex natural compositions are not caused by the absence of minor components from the model systems. Although no model system experimental data are included in the existing database for either MELTS or pMELTS, inclusion of such data are projected for the future (M. S. Ghiorso, pers. comm.). The pMELTS solidus is an improvement at both high and low pressures over that calculated from MELTS, and the solidus slope for pMELTS in the plagioclase-spinel lherzolite transition is close to the experimentally determined slope. It is hoped that this documentation of remaining differences will lead to further convergence in the future.